Naval Research Laboratory

Washington, DC 20375-5000

NRL Memorandum Report 6853

Hydrodynamic Target Response to an Induced Spatial Incoherence-Smoothed Laser Beam

M. H. EMERY AND J. H. GARDNER

Laboratory for Computational Physics and Fluid Dynamics

R. H. LEHMBERG AND S. P. OBENSCHAIN

Laser Plasma Branch

July 23, 1991

REPORT DOCUMENTATION PAGE

Form Approved
OMB No. 0704-0188

1. AGENCY USE ONLY (Leave blank)	2. REPORT DATE	3. REPORT TYPE AND DATES COVERED
	1991 July 23	INTERIM

4. TITLE AND SUBTITLE

Hydrodynamic Target Response to an Induced Spatial Incoherence-Smoothed Laser Beam

5. FUNDING NUMBERS

PE - 81103
PR - 8068
TA - 55
WU - 292601

6. AUTHOR(S)

M. H. Emery, J. H. Gardner, R. H. Lehmberg and S. P. Obenschain

7. PERFORMING ORGANIZATION NAME(S) AND ADDRESS(ES)

Naval Research Laboratory
Washington, DC 20375-5000

8. PERFORMING ORGANIZATION REPORT NUMBER

NRL Memorandum Report 6853

9. SPONSORING/MONITORING AGENCY NAME(S) AND ADDRESS(ES)

Department of Energy
Washington, DC 20545

10. SPONSORING/MONITORING AGENCY REPORT NUMBER

11. SUPPLEMENTARY NOTES

12a. DISTRIBUTION/AVAILABILITY STATEMENT

Approved for public release; distribution is unlimited.

12b. DISTRIBUTION CODE

13. ABSTRACT *(Maximum 200 words)*

One of the critical elements for high gain target designs is the high degree of symmetry that must be maintained in the implosion process. The induced spatial incoherence (ISI) concept has some promise for reducing ablation pressure nonuniformities to $\approx 1\%$. The ISI method produces a spatial irradiance profile that undergoes large random fluctuations on picosecond time scales but is smooth on long time scales. The ability of the ISI method to produce a nearly uniform ablation pressure is contingent on both temporal smoothing and thermal diffusion. In the startup phase of a shaped reactor-like laser pulse, the target is directly illuminated by the laser light and thermal diffusion is not effective at smoothing residual nonuniformities in the laser beam. During this period in the laser pulse, the target response is dominated by the initial shock generated by the laser pulse and the results indicate that this first shock can be the determining factor in the success or failure of the implosion process. The results of numerical simulations of several target/laser pulse designs which were investigated in an attempt to mitigate the impact of the initial shock structure stemming from the early temporal phase of an ISI-smoothed laser beam are presented. It is shown that "foam-like" layers, multiple laser wavelengths and shallow angles of incidence can sharply reduce the perturbation level stemming from the first shock.

14. SUBJECT TERMS	15. NUMBER OF PAGES
Induced spatial incoherence (ISI) Richtmyer-Meshkov Hydrodynamic target response	44
	16. PRICE CODE

17. SECURITY CLASSIFICATION OF REPORT	18. SECURITY CLASSIFICATION OF THIS PAGE	19. SECURITY CLASSIFICATION OF ABSTRACT	20. LIMITATION OF ABSTRACT
UNCLASSIFIED	UNCLASSIFIED	UNCLASSIFIED	UL

CONTENTS

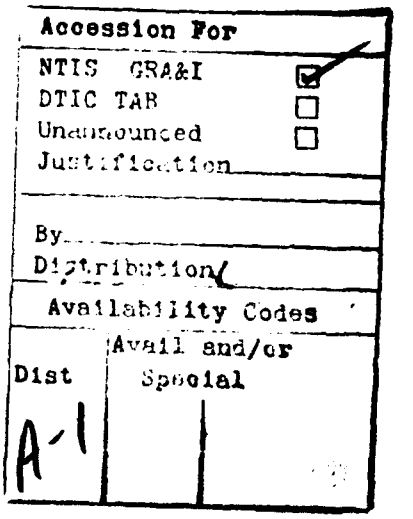

HYDRODYNAMIC TARGET RESPONSE TO AN INDUCED SPATIAL INCOHERENCE-SMOOTHED LASER BEAM

I. INTRODUCTION

One of the critical elements for high gain laser target designs is the high degree of symmetry that must be maintained in the implosion process. Asymmetries in the ablation pressure must be smaller than a few percent if high gain is to be achieved.[1] This places a severe requirement on the uniformity of the laser beam since thermal diffusion is only effective at reducing those spatial nonuniformities with scalelengths smaller than the separation distance between the absorption and the ablation region.[2] With short laser wavelengths, required for good laser-target coupling[3], thermal diffusion is ineffective at reducing all but the highest spatial frequency nonuniformities.

Recently, three techniques have been developed which show some promise for reducing ablation pressure nonuniformities down to $\approx 1\%$. These methods are based on the concept of slicing the laser light into small beamlets that are subsequently integrated at the target plane. The random phase plate (RPP) technique [4] slices the laser light into many beamlets with a transparent phase mask which randomly imposes a fixed phase shift of either 0 or π on each of the beamlets. These beamlets are overlapped onto the target plane by a focusing lens, resulting in a complicated interference pattern. The random phase relationship between the beamlets remains fixed in time; as a result, the focal interference pattern remains stationary. In the smoothing by spectral dispersion (SSD) technique,[5] the transparent phase mask is illuminated by periodic broadband light whose different spectral components sweep across the beam in cycles. This "color cycling" suppresses the

Manuscript approved May 10, 1991.

interference among most of the beamlets, although it does allow residual long scalelength structure due to interference among neighboring beamlets.

In the induced spatial incoherence (ISI) concept [6], a broadband laser beam (bandwith $\Delta\nu \gg 1/t_{pulse}$) is sliced into an array of small beamlets by an orthogonal pair of echelon structures which impose a time delay, Δt, at each step. If the delay increments are somewhat longer than the optical coherence time, $t_c = 1/\Delta\nu$, the beamlets become mutually incoherent. The beamlets are then overlapped onto the target by a lens of focal length f giving a smoothly varying far-field diffraction profile of total width $2f\lambda/D_1$, where D_1 is the echelon step size and λ is the laser wavelength. At any instant, the overlapped beamlets produce a complicated interference pattern; however, on time scales long compared to t_c, the interference pattern averages out, leaving only the smooth diffraction profile. If the hydrodynamic response time of the target (t_h) is much longer than the coherence time of the laser ($t_c \approx 1ps$), then the target will respond hydrodynamically only to the smooth time-averaged diffraction profile.

Numerical simulations of the time averaged intensity and ablation pressure profiles for a planar target indicate that an ISI-smoothed laser beam can result in a peak-to-valley deviation from the ensemble-averaged ablation pressure of less than 2%.[6] These results were obtained with a 3D numerical code (CHAOS), which evaluates the diffraction integral for an incident laser beam of arbitrary aberration. Quasi-steady state conditions were assumed for the target and plasma and thermal smoothing effects were modeled with a heuristic "cloudy day", exp(-kd), approximation with an assumed absorption to ablation distance

d = 50 μm with 0.527 μm laser light.[6] This relatively good pressure uniformity would be expected as the dominant mode for the time averaged ISI-spectrum for the chosen beam parameters (averaged over 100 t_c) has a scalelength of O(50 μm). Thus thermal diffusion would smooth out residual asymmetries with scalelengths of this order and smaller.

Transverse thermal conduction is effective at minimizing irradiation nonuniformities as long as there is sufficient distance, "d", between the laser absorption region and the ablation region. This is difficult to achieve during the *initial phase* of a reactor-like laser pulse for which the laser intensity is $\leq 10^{13} W/cm^2$. The low intensity of this initial phase is required in order to keep the fuel on a low adiabat. Thermal smoothing is not effective for the first several nanoseconds of the pulse as the absorption-to-ablation distance is only a few microns, or less, with 1/4 μm laser light. This implies that the shock structure generated during the start-up phase of the laser pulse will mirror the laser nonuniformities. The shocks produced during the start-up phase can be the determining factor in the success or failure of the implosion process. The start-up problem is the subject which we address in this paper. We present the results from a series of numerical simulations using the FAST2D Laser Matter Interaction Model; and, in particular, we investigate the impact of a shaped, reactor-like, ISI-smoothed laser beam on solid DT targets. In the next section we discuss the numerical model, the results are presented in Section III, followed by the summary and conclusions.

II. MODEL

The numerical results are generated with the FAST2D Laser Matter Interaction Model. This is a fully two-dimensional, Cartesian, fully compressible hydrodynamics code with a sliding Eulerian grid with variable grid spacing. The grid spacing is typically 0.25 μm for 15 - 20 zones on either side of the ablation layer and increases uniformly to 2 - 10 μm for most of the rest of the grid. The grids at the outer boundaries of the computational mesh are stretched to 200 - 300 μm. The grid slides with the average velocity of the accelerated foil so that the ablation front remains approximately centered in the finely zoned region thus reducing convective errors.

The time-dependent equations for the continuity of mass, momentum and total energy are integrated numerically with sliding-zone flux-corrected- transport (FCT).[7] FCT solves the continuity equations for the fluxes relative to moving zone boundaries. The overall scheme is second-order accurate and no artificial viscosity is explicitly required to maintain numerical stability. Mass, momentum and energy are both locally and globally conserved.

Thermal conduction is incorporated in a single-temperature model using a semi-implicit solution of the two-dimensional, classical, non-linear thermal conduction equation based on the model of Spitzer and Härm.[8] The laser energy is absorbed by classical inverse bremsstrahlung absorption with a resonant dump at the critical density. For most of the results presented here the laser light is at normal incidence. In order to investigate the role of the angle of incidence of the laser beam, we have incorporated a ray trace model[9] based

on one developed by Delettrez and Grandjouan.[10] The fluid equations are closed with a real equation of state.

The equations of state express the pressure P = F(e,ρ) and the temperature T = G(e,ρ), where e is the energy and ρ is the density, and are based on the solid material models used in the analytic model (ANEOS) in the CHARTD code.[11] The model includes the effects of solid material, Fermi-temperature and fractional ionization. This includes the effect of a Debye-Grüneisen model near solid density and the scheme transitions smoothly from a Thomas-Fermi-Dirac model for degenerate electrons at high density and low temperature to a Saha equiblibrium model at high temperature and low density.

In FAST2D, the ISI laser intensity is given by[5]

$$I(y,t) = \langle I(y) \rangle P(t) |S(y,t)|^2, \tag{1}$$

where ⟨ I(y) ⟩ is the average spatial profile (assumed constant), P(t) is the slow time varying pulse envelope and S(y,t) describes the statistical behavior of the rapidly varying stochastic optical field :

$$S(y,t) \equiv \frac{1}{(N_s)^{1/2}} \sum_{n=1}^{N_s} F(t - n\Delta t_1) e^{i\phi_n} e^{i4\pi n y / d_{00}}. \tag{2}$$

Here, N_s is the number of echelon steps, Δt_1 is the delay increment between two adjacent steps, ϕ_n is an array of N_s statistically independent random phases, d_{00} is the

zero - to - zero distance (spot size) and $F(t\text{-}n\Delta t_1)$ is the stochastic complex optical field amplitude:

$$F(t\text{-}n\Delta t_1) \equiv \frac{1}{\sqrt{2}}[F_r + iF_i],$$

$$\langle F \rangle = 0, \langle |F|^2 \rangle = 1.$$

Expanding the sum over the number of echelon steps, we obtain :

$$I(y,t) = \frac{IP(t)}{N_s} \sum_{n=1}^{N_s} |F(t - n\Delta t_1)|^2 +$$

$$\frac{IP(t)}{N_s} \sum_{j=1}^{N_s-1} \sum_{\substack{k=1 \\ k>j}}^{N_s} \{(F_{rj}F_{rk} + F_{ij}F_{ik})cos[\phi_k - \phi_j + (k-j)4\pi y/d_{00}] \qquad (3)$$

$$+(F_{ij}F_{rk} - F_{rj}F_{ik})sin[\phi_k - \phi_j + (k-j)4\pi y/d_{00}]\}.$$

F_r and F_i are independent arrays of real numbers satisfying Gaussian statistics, and $\langle F_r \rangle = \langle F_i \rangle = 0$; $(F_r)_{rms} = (F_i)_{rms} = 1$.

These arrays are regenerated every numerical time step and the numerical time step is forced to remain $\leq t_c$. As noted above, the spot size is given by $d_{00} = 2\,f\,\lambda/D_1$, where f is the focal length, λ is the laser wavelength and D_1 is the step size. The length of the n^{th} transverse mode in the ISI spectrum is given by $\lambda_n = f\,\lambda/(nD_1)$. The longest mode is $d_{00}/2$ and the shortest mode is $d_{00}/(2N_s)$. FAST2D employs periodic boundary conditions in the direction transverse to the laser propagation, thus, computationally, the longest mode represented is $d_{00}/2$; i.e., half of the spot size. The laser beam is assumed

to have a flat spatial profile; i.e., $\langle I(y) \rangle$ = constant. The numerical results are presented in the next section.

III. RESULTS

For most of the results presented here, we modeled the laser profile with a 20 x 20 echelon array with $d_{00} = 320\ \mu m$ and a laser coherence time $t_c = 1$ ps. The laser wavelength is 0.264 μm. This corresponds to a lens with an $F_{number} = 32$. The laser spot is flat over the distance d_{00}. The transverse dimension is 160 μm, represented by 80 zones, and there are 120 zones in the longitudinal direction. The ISI mode spectrum ranges between 8 μm and 160 μm. This compares favorably with the envisioned reactor-like parameters : $F_{number} \approx 30$, $d_{00} = 600\ \mu m$ and a 60 x 60 echelon array. These conditions produce an ISI spectrum ranging between 5 μm and 300 μm.

The instantaneous incident ISI laser profile exhibits large amplitude randomly fluctuating structures as shown in Figure 1. Here is plotted the instantaneous incident laser intensity (in arbitrary units) versus the transverse dimension (in microns) at four arbitrary times. The long time average behavior (100 t_c) still exhibits some residual structure as shown in Figure 2. After 100 ps, the laser intensity has a root-mean-square deviation $\sigma_{RMS} = 0.10$ with a maxmimum amplitude variation of 1.7:1, or ±25%. The RMS deviation for the incident light follows a $(t_c/t)^{1/2}$ dependence.[5] This is illustrated in Figure 3 which shows the time averaged incident laser profile after 500 t_c and after 1000 t_c. After 1 ns, $\sigma_{RMS} = 0.037$ with a maximum amplitude variation of ±8.6%

These residual structures can be reduced in magnitude by lateral thermal smoothing as long as the distance between the ablation region and the laser absorption region is larger than the scalelengths of the residual laser asymmetries. To test this hypothesis, we generated a moderately long scalelength plasma with a "perfect" laser beam before impacting the target with an ISI-smoothed laser beam. The laser pulse has a 2 ns Gaussian rise to 5 x 10^{12} W/cm^2 after which it has a power law dependence ($t^{-5/4}$) which peaks at 5 x 10^{14} W/cm^2 at 13 ns and is then held constant. The laser light is spatially uniform until 6 ns, at which time the ISI spectrum is "turned on". At this time the distance between the ablation and critical surfaces is $\approx 1\mu m$; the distance between the ablation and 1/4 critical surfaces is $\approx 15\mu m$. Nearly all of the laser energy is absorbed between the 1/4 critical density and critical density surfaces. Figure 4 shows the isodensity contours and a 2D perspective plot of the mass density of an 80 μm thick CH target at 16 ns. The target is quite uniform well into the rapid acceleration phase. The mass perturbation at 16 ns is $\Delta m/m \approx 0.2\%$. It is evident that transverse thermal conduction effectively reduces the long time average residual structure inherent in the ISI laser beam profile when there is sufficient separation between the laser absorption region and the ablation region.

These density profiles are to be contrasted with the case of a "frozen-in" 4:1 sinusoidal laser asymmetry which is illustrated in Figure 5. The initial conditions are the same as the ISI case; i.e., the laser profile is uniform until 6 ns at which time the target is illuminated with the asymmetric beam. At 9.5 ns, 3.5 ns after the asymmetric beam is "turned on", the target is severely distorted with a 13 μm depression which mirrors the laser asymmetry.

Note that this is solely due to the differential mass ablation rate and ablation pressure asymmetry. There is very little target acceleration at this point in the laser pulse and the Rayleigh-Taylor[12,13] (RT) instability is not playing a role here.

A similar result is obtained with an ISI-like beam with zero bandwidth. In this case, at 6 ns, the uniform laser profile shifts to a "frozen-in" ISI-profile. A plot of the incident intensity is shown in Figure 6. The target density contours are shown in Figure 7 at 11 ns. The target is markedly distorted at this time and a portion of this growth, $\approx$ 1 e-folding, is due to the RT instability as the target has begun to accelerate at this point in the pulse. At 6 ns, the ablation-to-absorption distance is not large enough to thermally smooth out the large scalelength asymmetries resulting from the zero bandwidth ISI case.

The ability of the ISI concept to result in a smooth ablation pressure is based on a combination of temporal smoothing (over 100's of t_c) and transverse thermal smoothing. Transverse thermal conduction is effective at minimizing the long time average residual structure inherent in the ISI-smoothed laser beam as long as the sound transit time between the laser absorption region and the ablation front is greater than the ISI averaging time (100 - 200 t_c). Unfortunately, this necessitates a long scalelength, uniform plasma in the laser absorption region. This is difficult to achieve with a reactor-like shaped laser pulse which may entail a long, low intensity "foot" prior to the main driving beam. The laser intensity can be $\leq 10^{13} W/cm^2$ for nearly 80% of the temporal length of the pulse. A canonical power law shaped laser pulse is shown in Figure 8. After a 1/2 ns Gaussian rise to 10^{12} W/cm^2, the pulse has a $t^{-5/4}$ dependence to 3 x 10^{14} W/cm^2 at 15 ns after which

the laser intensity is held fixed. This pulse is designed so that the first shock breaks out through the rear of the target as the laser intensity reaches its maximum value.

The severity of the thermal smoothing problem is illustrated in Figure 9, where the distances between the ablation surface and the critical surface (solid line) and the ablation surface and the quarter critical surface (dashed line) are plotted as a function of time for the above laser pulse. For 2/3 of the laser pulse, the critical surface is less than 1/2 μm from the target surface.

The initial pulse sends an $\approx$ 2/3 Mb shock through the 330 μm thick DT target which keeps the fuel on a low adiabat. The ablation pressure history and the peak target density history are shown in Figure 10. The target density is initially compressed by a factor of 4, from 0.2 to nearly 0.8 gm/cm^3. For a strong shock, the compression ratio is given by $(\gamma + 1)/(\gamma - 1)$ where γ is the ratio of specific heats, $\gamma \approx 5/3$ for DT. At the peak of the laser pulse, the target density has been compressed by a factor of over 30. The ablation pressure at this time is 45 Mbar. The velocity history of the target is shown in Figure 11. The initial shock imparts a velocity of 1.5 x 10^6 cm/s to the target. The target velocity remains nearly constant until $\approx$ 12 - 13 ns, at which time the target begins to rapidly accelerate as a result of the increasing laser intensity. The target velocity is 7.5 x 10^6 cm/s at 15 ns and the acceleration is 8.5 x 10^{15} cm/s^2. At this point the target has traveled 300 μm. It is the mass variations near the peak of the laser pulse which will provide the seeds for the RT growth during the acceleration phase. For a target to implode uniformly, the mass variations at this point must be $\ll$ 1%. Note that the target attains a sizeable

acceleration between the 12 - 15 ns time interval and any residual mass perturbations can undergo 1 - 2 e-foldings of RT growth during this time period. For the results presented below, the ISI spectrum is in effect from the beginning of the pulse.

The isodensity contours for a 330 μm thick DT target illuminated with a 0.264 μm ISI laser beam is shown in Figure 12 at t = 12 ns. At this time the target mass variation $(\Delta(\rho r)/\langle \rho r \rangle)$ is 22%. Early in the laser pulse, the laser energy is deposited directly onto the target surface. The highly nonuniform nature of the ISI beam results in spatially and temporally nonuniform shocks traversing the target. The target surface, itself, is perturbed and as the shock passes through the target it leaves residual mass perturbations in its wake. This is apparent from Figure 13 where plots of the target mass variation $(\Delta(\rho r)/\langle \rho r \rangle)$ at 0.4, 0.6, 0.8 and 1.0 ns show rapid variations in the mass perturbations. The same phenomenon is discernable in 2D perspective plots of the mass density, Figure 14. As the shock traverses the dense target, perturbations on the shock front eventually dissipate and the shock front straightens out. This occurs because, relative to the average velocity of the shock front, the leading portion of the shock, the crest, is divergent and thus slows down; whereas, the trailing portion, the trough, is convergent and thus speeds up. In addition, once the sound transit time between the absorption region and the ablation region becomes greater than the ISI averaging time, the rapidly varying ISI laser beam no longer perturbs the target. The residual mass variations, however, persist. Mass density plots at 3.0 and 3.2 ns shown little difference in the mass variation on the target surface,

see Figure 15. These residual variations grow linearly in time, in a Richtmyer-Meshkov[14]-like manner, as the target drifts with a nearly constant velocity. Figure 16 shows a 2D surface plot of the integrated mass density (ρr) as a function of time. ρr is integrated from the rear of the target to the ablation front for each transverse coordinate. The residual perturbations begin to grow after about 1 ns. $\Delta\rho r$ between line-outs taken along paths 1 and 2 and along paths 2 and 3 (see arrows in Figure 16) are plotted as a function of time in Figure 17. The initial growth is linear in time.

That this should be the case is clear from the theoretical expression for RM growth[15],

$$\dot{\eta} = (2\pi/\lambda)\eta_o A' U_i (1 - U_i/U_s), \tag{4}$$

where η_o is the initial amplitude, λ is the wavelength, U_s is the velocity of the shock wave, U_i is the velocity imparted to the interface, the Atwood number $A' = (\rho'_+ - \rho'_-)/(\rho'_+ + \rho'_-)$, where ρ'_+, ρ'_- are the densities at the interface just after passage of the shock. For the parameters investigated here, A' is O(1), and

$$\Delta\eta/\eta_o = (2\pi/\lambda)U_i(1 - U_i/U_s)\Delta t. \tag{5}$$

The appropriate time increment is the shock breakout time, $\Delta t = \Delta x/U_s$, where Δx is the target thickness. From the mass conservation equation, $U_i/U_s = (1 - \rho_d/\rho_u)$,

where $\rho_d(\rho_u)$ is the density downstream (upstream) of the shock. For a strong shock, $\rho_d/\rho_u = (\gamma-1)/(\gamma+1) = 1/4$, for DT, and

$$\Delta\eta/\eta_o = 3\pi/(8\lambda)\Delta x. \tag{6}$$

Thus for perturbation wavelengths of 40 - 50 μm and target thicknesses of 300 μm, small initial perturbations can grow an order of magnitude in size solely as a result of shock driven growth, well before the target acceleration phase. This is equivalent to over 2 e-foldings of growth. This growth will occur whether the perturbations stem from laser imperfections or target surface imperfections[16]. The problem is exacerbated by thick targets and strong shocks.

Further evidence for the claim that the initial shock structure is the determining factor in the subsequent evolution of the target can be gained from the case in which the ISI spectrum is "turned off" after 3 ns; i.e., the laser profile is modeled as being perfectly uniform for t $\geq$ 3ns. There is essentially no difference in the amplitude of the mass perturbations, later in time, for this case as compared to the case in which the ISI spectrum is "on" throughout the whole pulse. In addition, a case was run in which the ISI spectrum is averaged over 500 t_c and then held fixed (see Figure 3a) during the shaped power law laser pulse. After 3 ns, the amplitude of the mass perturbation is $< 10\%$ smaller than for the full ISI spectrum case.

Although it appears that a long pulse ISI laser beam may severely perturb an ICF target, this should be contrasted with the impact of a temporally equivalent laser pulse with a "frozen-in" 4:1 sinusoidal asymmetry. In this case, the laser asymmetry is imposed at t = 0 and the mass variation is greater than 2:1 at 8 ns.

Several target designs were investigated in an attempt to mitigate the impact of the initial shock structure stemming from the early temporal phase of the ISI laser beam. In one case, a 180 μm thick solid DT target with a 100 μm thick "foam-like" DT layer was used. This "foam-like" layer does not contain any voids and pore compaction is not modeled. The "foam-like" layer is simply low density DT, $\rho_{foam} = 0.08 gm/cm^3$. This layer reduces the perturbation on the shock front to some degree before the shock impacts the frozen DT target. The mass variation at 15 ns is 21% with 0.264 μm ISI laser light.

The ablation to absorption distance can be increased by using longer wavelength laser light which would also result in an increase in the amount of thermal smoothing. However, longer wavelength laser light implies poorer laser-target coupling and reduced efficiency.[3] By combining long wavelength laser light at the beginning of the pulse with short wavelength laser light during the compression and acceleration phases, thermal smoothing would be enhanced during the early phase of the pulse and laser-target coupling would be enhanced during the acceleration phase. Using the same multilayer target discussed above, the first 8 ns of the laser beam is modeled as 1.054 μm ISI laser light (t_c=1 ps) which then smoothly evolves, over 1.5 ns, to 0.264 μm ISI laser light (t_c=1 ps) for the rest of the laser pulse. At 15 ns, $\Delta(\rho r)/\langle \rho r \rangle = 4\%$. The perturbation amplitude at this time includes $\approx$

1.5 e-foldings of RT growth. At 12 ns, $\Delta(\rho r)/\langle\rho r\rangle = 0.9$ %. Modeling the first 8 ns of the 1.054 μm beam as being perfectly uniform results in a mass variation of only 1.8% at 15 ns (0.4% at 12 ns). These perturbation levels are still too large to enable the target to implode uniformly. The isodensity contours for the second of these two cases is shown in Figure 18.

The ablation to absorption distance also depends on the angle of incidence of the laser. The position of the turning point for the laser light is given by $r_t = r_c + 2L\ ln(\cos(\theta))$, where r_c is the position of the critical surface, L is the density scalelength and θ is the angle of incidence of the laser. Since it is the early time impact of the laser which is perturbing the target, L must be nonzero in order that there be any increase in thermal smoothing. In the absence of a "perfect" laser beam, a uniform blowoff plasma could be generated by coating the target with a thin (O(few 100 $\AA$) high-Z material and striking the target with a very short burst of x-rays. We have approximated this interaction by depositing 1/4 J of energy directly onto the surface of a frozen DT target during a 250 ps FWHM pulse. The target is 330 μm thick. This energy pulse produces a very weak shock, O(10's of kbar), and at 10 ns after the "x-ray flash", the density scalelength, at critical density for 1/4 μm laser light, is $\approx 100\mu m$. The density profile at this time is shown in Figure 19. The target is then illuminated with a 0.264 μm ISI - smoothed laser beam at a 30° angle of incidence (with respect to the normal). For this case, the laser pulse has a 5 ns Gaussian rise to an intensity of 10^{12} W/cm^2 which then evolves into a power law pulse which peaks at 3 x 10^{14} W/cm ^{2} at 15 ns. A plot of the rays incident at an angle of 30° at the peak of the laser

pulse is shown in Figure 20. The turning point of the rays is just outside of the critical surface and the plasma continues to absorb energy from the rays until each ray contains < 1% of its initial energy. The maximum mass variation of the target, $\Delta(\rho r)/\langle\rho r\rangle$, is 4.8 % at 15 ns. The isodensity contours at 15 ns are shown in Figure 21. The mass perturbations are larger than the layered, multiple laser wavelength cases, but significantly smaller than the nonlayered, normal incident cases.

IV. SUMMARY AND CONCLUSIONS

We have numerically simulated the hydrodynamic response of a series of thick, frozen DT targets directly illuminated with an ISI-smoothed, ICF reactor-like, shaped laser pulse. Studies of the "start-up" problem and the impact of the first shock on subsequent target development are important for both target design and pulse shaping. The results indicate that the first shock can be the determining factor in the success or failure of the implosion process. This is the case whether the perturbations on the shock front stem from laser imperfections, as investigated here, or surface imperfections.[16] A perturbed shock front leaves residual mass variations in its wake as it transits the target. These mass variations are the seeds for the subsequent Rayleigh-Taylor growth which will occur during the acceleration phase of the laser pulse. For a strong shock and thick targets, these mass variations can undergo $\approx$ 2 e-foldings of growth before the target begins the main acceleration phase.

The ability of the ISI technique to provide nearly uniform ablation pressures is contingent on both temporal averaging, over 100's of coherence times, and thermal diffusion. With a moderate scalelength, uniform, preformed plasma, an ISI-smoothed laser beam can

accelerate the target uniformly. Under similar initial conditions, asymmetric laser beams and beams with echelon steps but zero bandwidth can severely perturb the target. In the latter two cases there is no temporal averaging, and thermal diffusion is not large enough to smooth out the intensity perturbations.

In the absence of a "perfect" laser beam and/or a uniform preformed plasma, some means may be needed to mitigate the impact of the first shock from a shaped reactor-like laser pulse. We have shown that cold, low density layers, multiple wavelength lasers and shallow angles of incidence can all significantly reduce the perturbations stemming from an imperfect laser beam. Some combination of the above target designs may be needed in order to uniformly implode a thick ICF capsule. It should be noted that these designs may reduce the overall efficiency of the implosion process. Finally, it may be possible to compress the target adiabatically - without any shocks. This could entail a very long (50 - 100 ns), slowly rising laser pulse. A laser pulse of this shape would generate kilobar-like pressures in the target, and thus compressive stress, shear stress, melt and pore compaction, in the case of foams, become important. We are presently modifying our EOS model in order to more accurately simulate these physical phenomena.

ACKNOWLEDGEMENTS

One of us (MHE) would like to gratefully acknowledge Dr. J. Delettrez for providing us with information concerning his ray trace model developed at CECAM. This formed the basis of the ray trace model used here. This work was supported by the US Department of Energy and the Office of Naval Research.

REFERENCES

1. S. E. Bodner. J. Fusion Energy **1**, 221(1981).

2. M. H. Emery, J. H. Orens, J. H. Gardner, and J. P. Boris, Phys. Rev. Lett. **48**, 253(1982).

3. J. H. Gardner, and S. E. Bodner, Phys. Rev. Lett. **47**, 1137 (1981).

4. Y. Kato, K. Mima, N. Miyanaga, S. Arinaga, Y. Kitagawa, M. Nakatsuka, and C. Yamanaka, Phys. Rev. Lett. **53**, 1057(1984).

5. S. Skupsky, R. W. Short, T. Kessler, R. S. Craxton, S. Letzring, and J. M. Soures, J. Appl. Phys. **66**, 3456 (1989).

6. R. H. Lehmberg and S. P. Obenschain, Opt. Commun. **46**, 27(1983); R. H. Lehmberg, A. J. Schmitt, and S. E. Bodner, J. App. Phys. **62**, 2680 (1987).

7. J. P. Boris and D. L. Book, Methods Comput. Phys. **16**, 85 (1976).

8. L. Spitzer and R. Härm, Phys. Rev. **89**, 977 (1953).

9. M. H. Emery and John H. Gardner, Bull. Am. Phys. Soc. **35**, 1969 (1990).

10. J. Delettrez and N. Grandjouan, CECAM Report of Workshop on Rayleigh-Taylor Instabilities, Thermal Smoothing and Interactions in Laser Plasmas, (CECAM, Orsay, 1988) p. 24.

11. S. L. Thompson and H. S. Lauson, Sandia Laboratory Report No. SC-RR-71 0714, 1972 (unpublished). (See National Technical Information Service document no. SC-RR-71 0714 (Improvements in the CHART D Radiation-Hydrodynamic Code III, by S. L. Thompson and H. S. Lauson). Copies may be ordered from the National Technical Information Service, Springfield, VA 22161. The price is $23.00 plus a $3.00 handling fee. All orders must be prepaid.)

12. Lord Rayleigh, *Theory of Sound*, 2nd. ed. (Dover, New York, 1945, Vol. 2); G. I. Taylor, Proc. R. Soc. London Ser. **A 201**, 192 (1950).

13. C. P. Verdon, R. L. McCrory, R. L. Morse, G. R. Baker, D. I. Meiron, and S. A. Orszag, Phys. Fluids **25**, 1653 (1982); M. H. Emery, J. H. Gardner, and J. P. Boris, Phys. Rev. Lett. **48**, 677 (1982), and Phys. Rev. Lett. **56**, 1757(E) (1986).

14. R. D. Richtmyer, Commun. Pure Appl. Math. **13**, 297 (1960); Ye. Ye. Meshkov, NASA Technical Translation NASA TT F-13, 074 (1970).

15. G. H. Markstein, J. Aerosol. Sci. **24**, 238 (1957).

16. M. H. Emery and J. H. Gardner, Bull. Am. Phys. Soc. **34**, 2114 (1989).

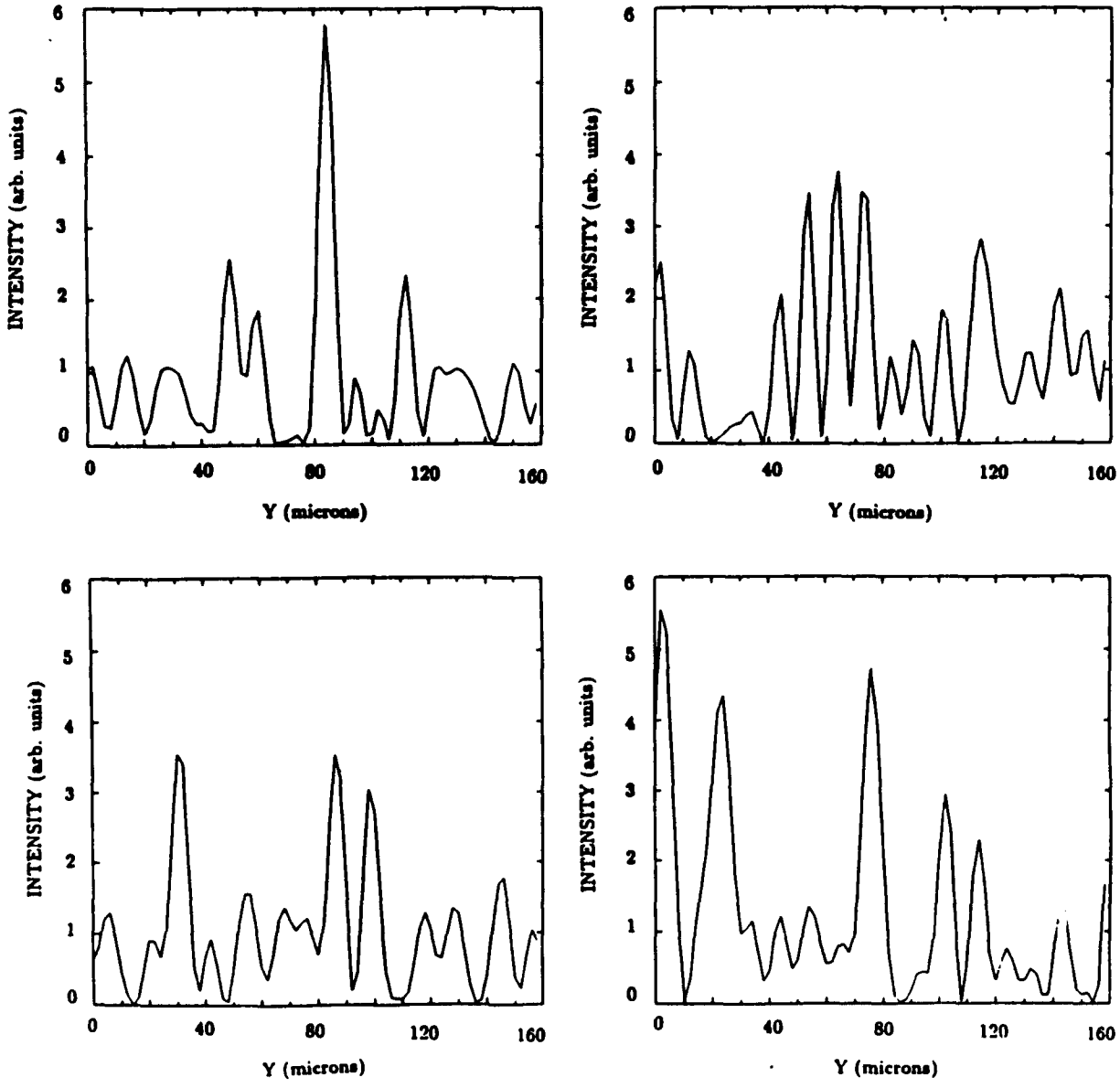

1. Plot of the instantaneous incident ISI laser intensity (arbitrary units) versus the transverse dimension (in microns) at four different times.

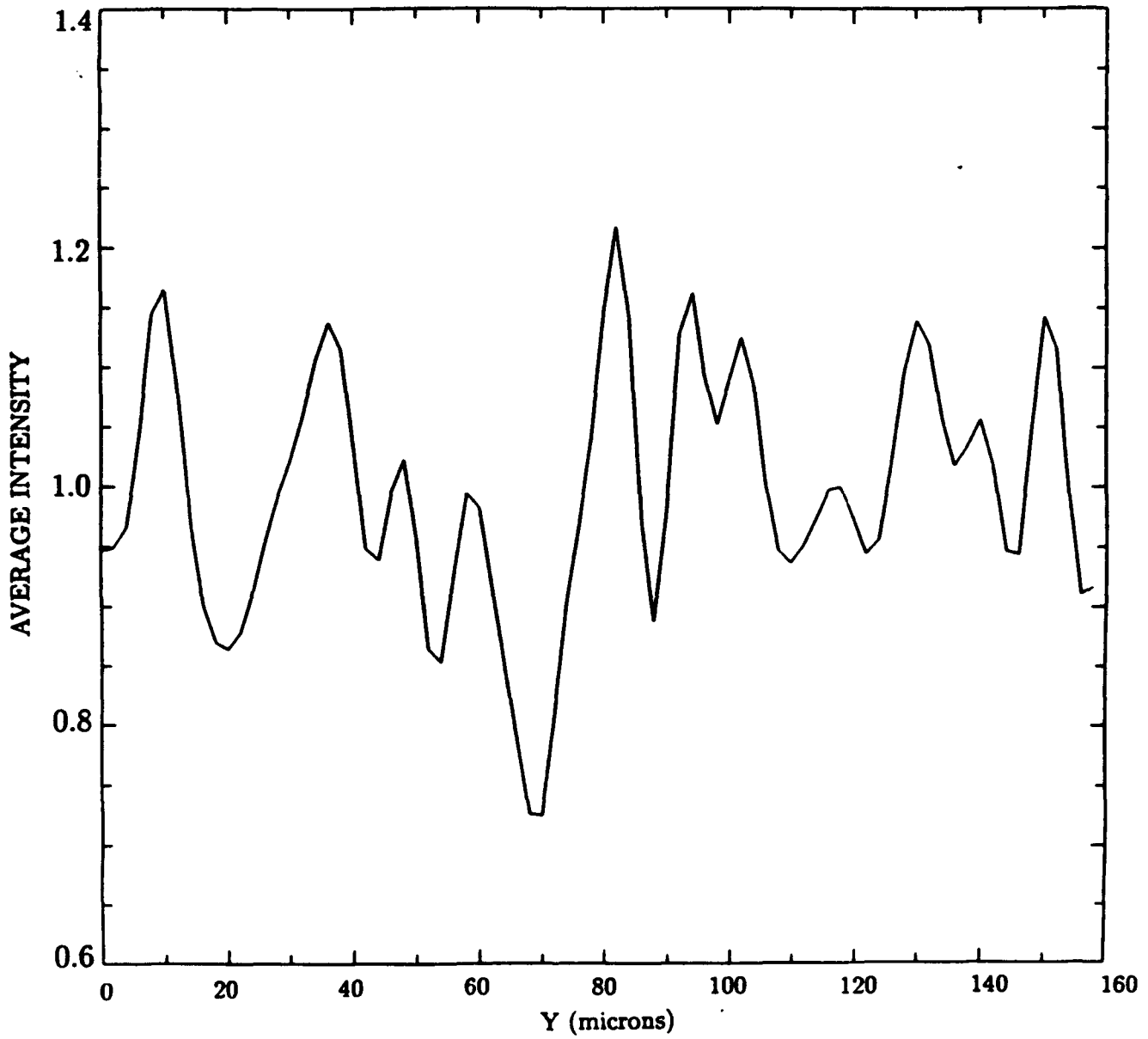

2. Plot of the laser intensity which has been averaged over 100 coherence times. The rms variation is 10%.

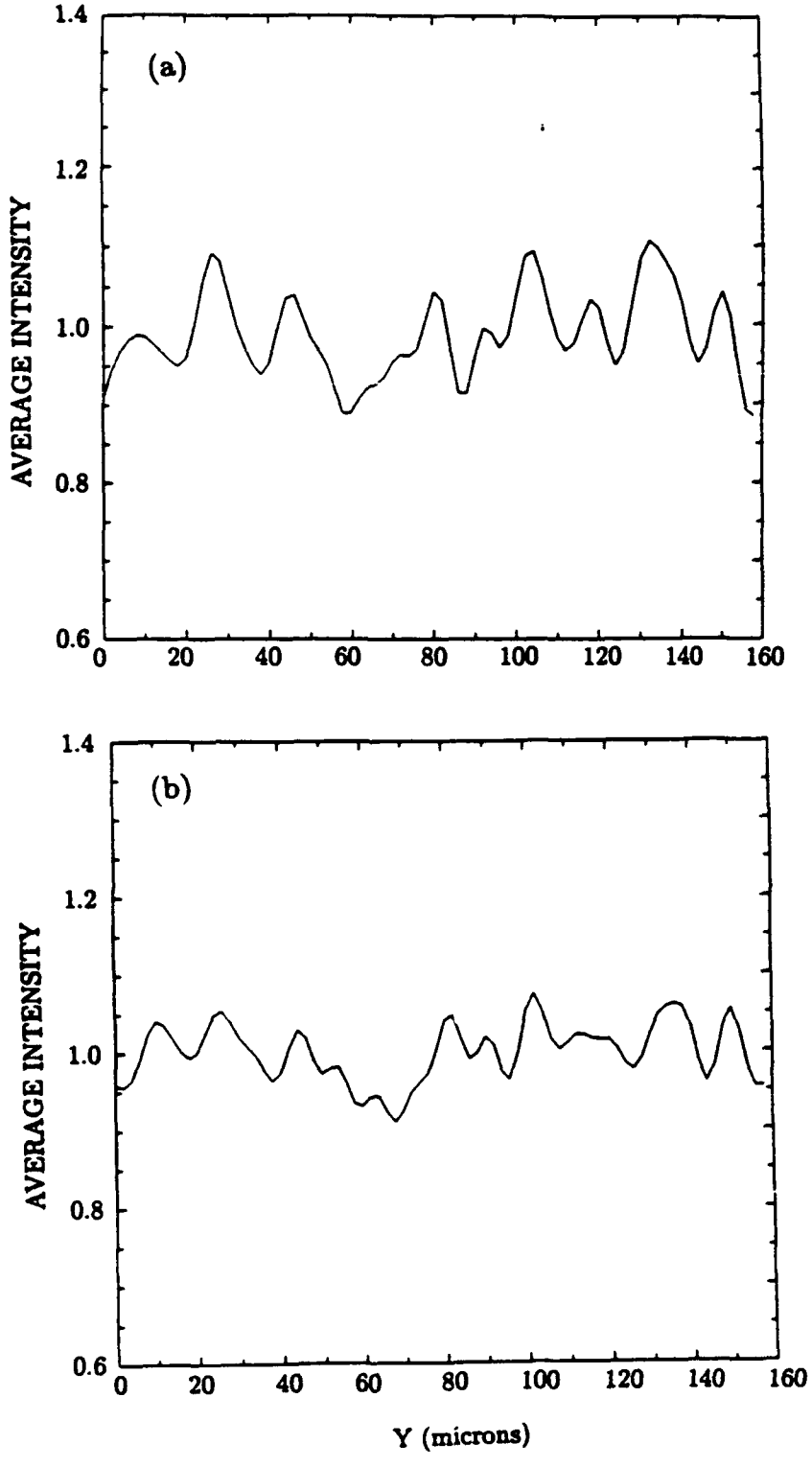

3. a) Plot of the laser intensity profile averaged over 500 coherence times, $\sigma_{RMS} = 0.045$.
b) Laser intensity profile averaged over 1000 coherence times, $\sigma_{RMS} = 0.037$.

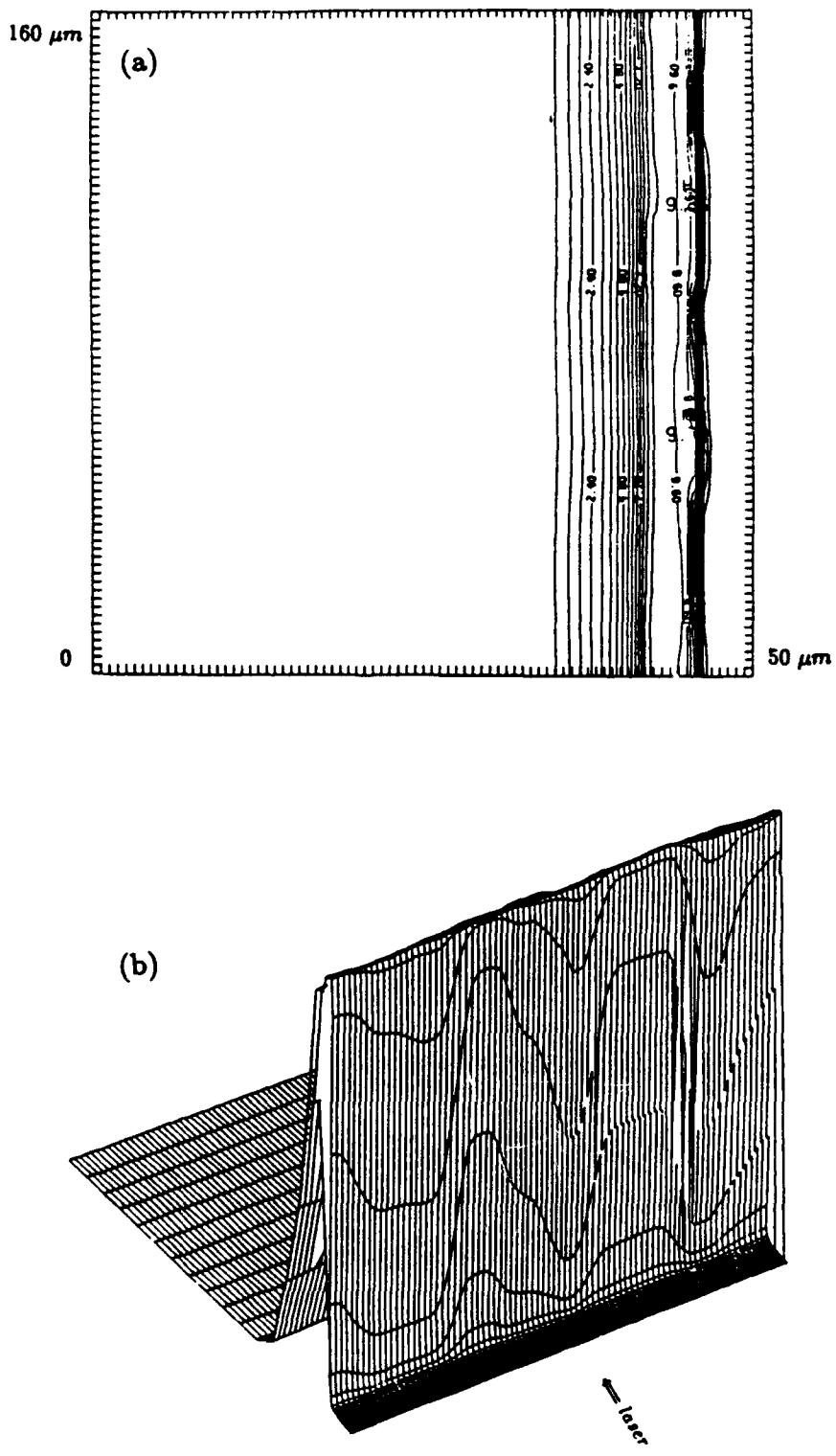

4. Isodensity contours (a) and a 2D perspective plot of the mass density (b) of an 80 μm thick CH target at 16 ns. The transverse dimension is 160 μm. The horizontal dimension is 50 μm. The laser is impacting the target from the right (a) and front (b).

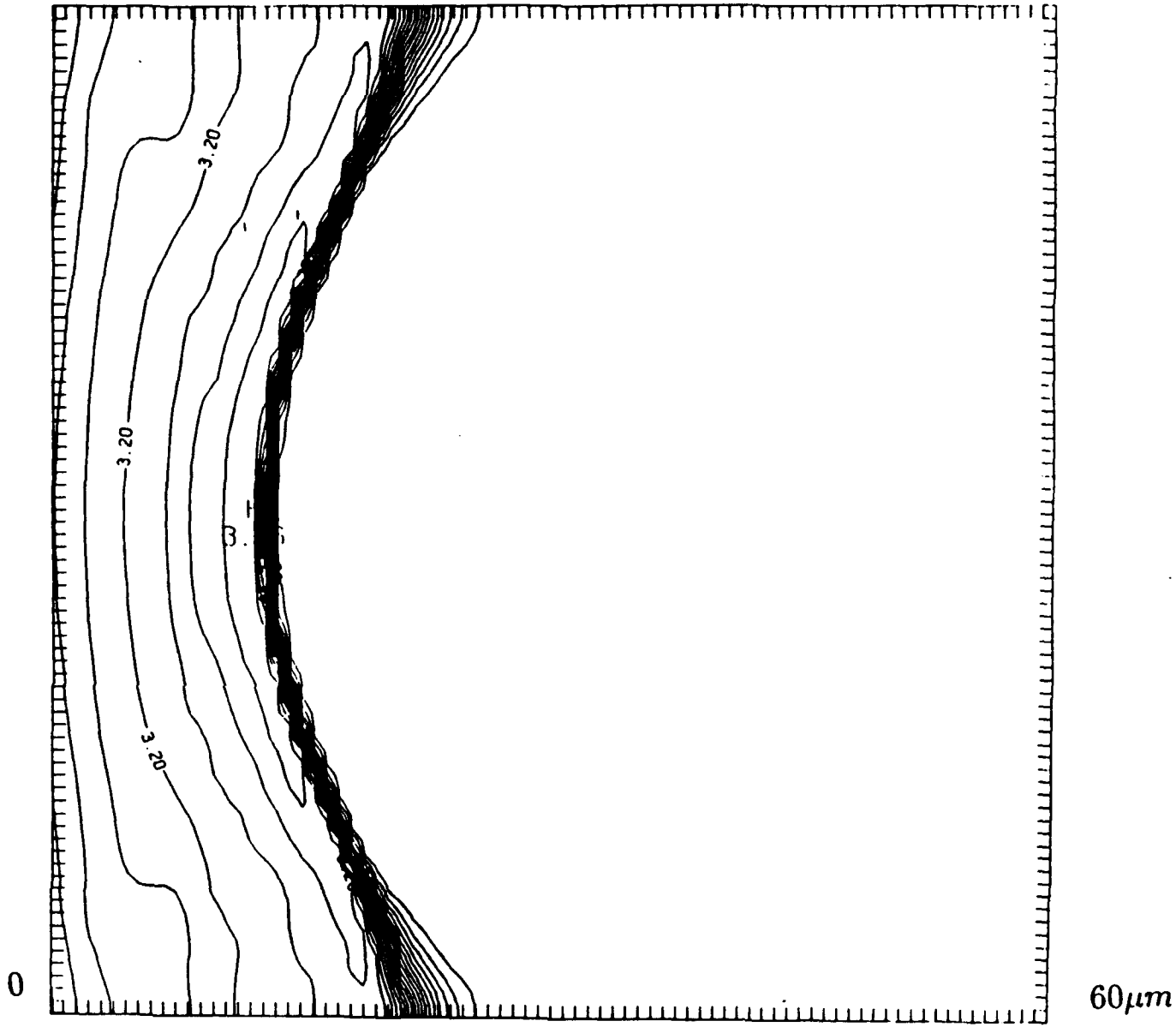

5. Isodensity contours of an 80 μm thick CH target impacted with a laser with an imposed 4:1 sinusoidal asymmetry. The time is 9.5 ns, the transverse dimension is 160 μm and the horizontal dimension is 60 μm.

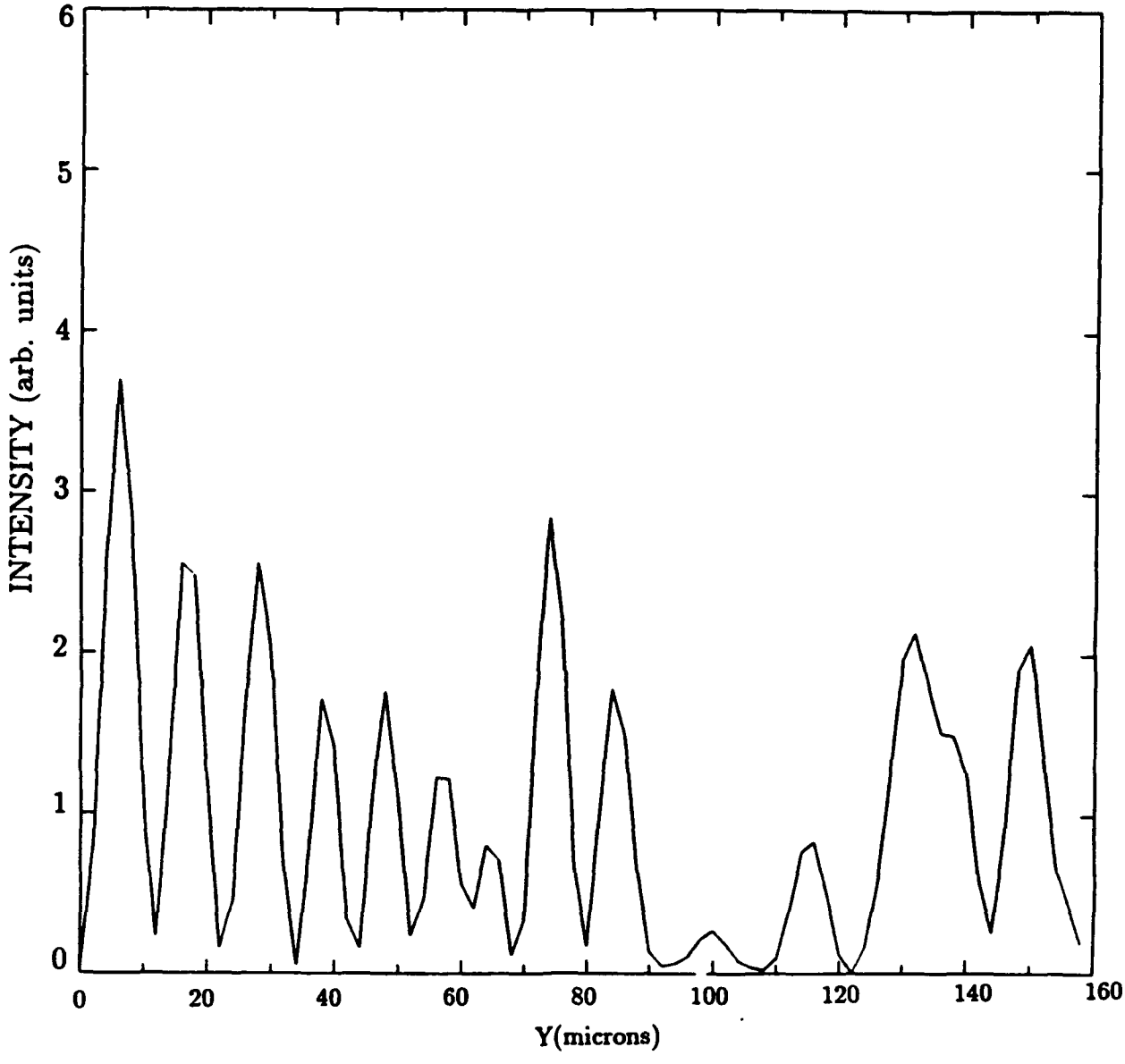

6. A plot of the incident intensity for an ISI beam with zero bandwidth.

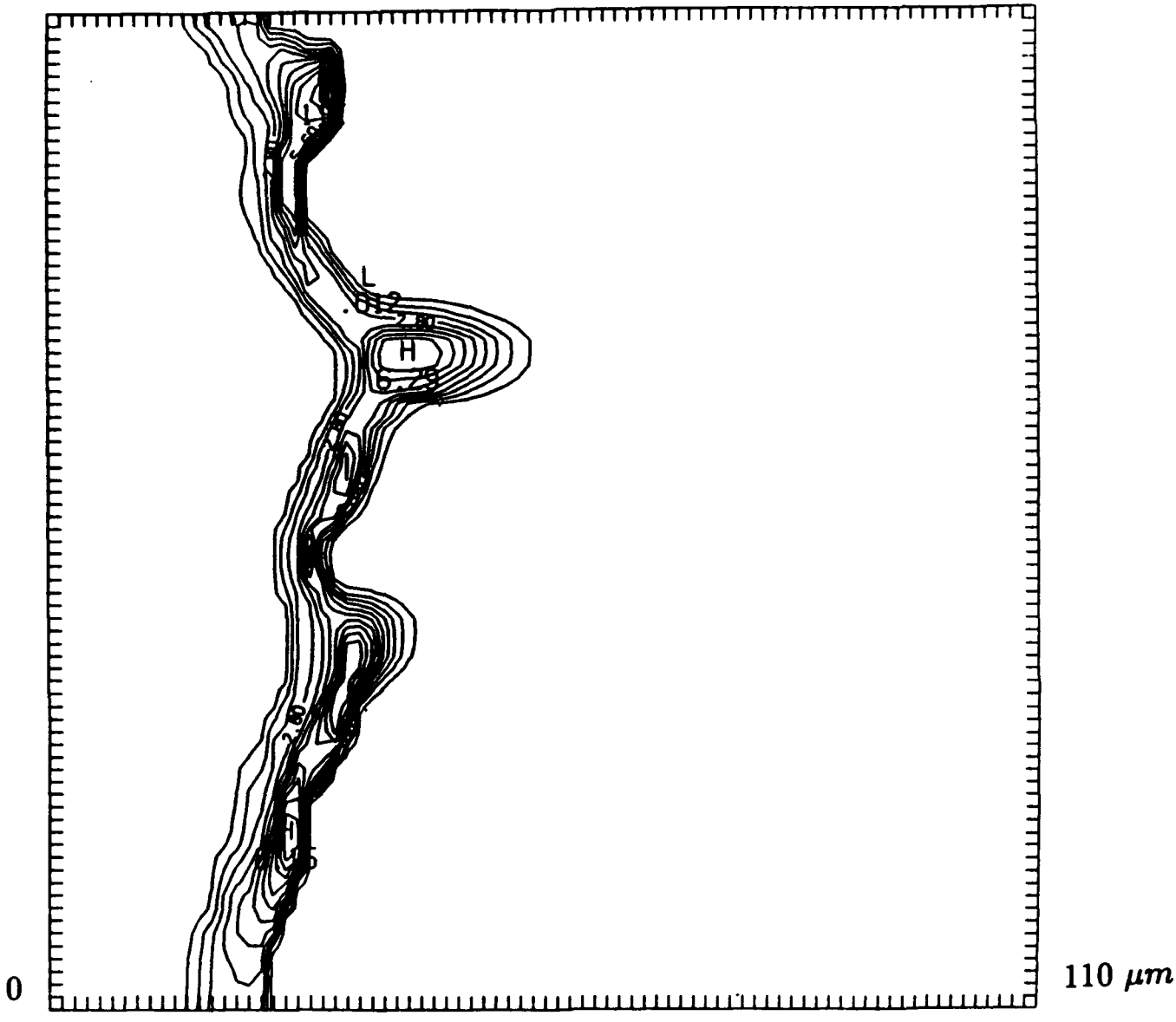

7. Isodensity contours of an 80 μm thick CH target impacted with the zero-bandwidth ISI laser profile illustrated in Fig. 6. The time is 11 ns and the horizontal and transverse dimension are 110 and 160 μm respectively.

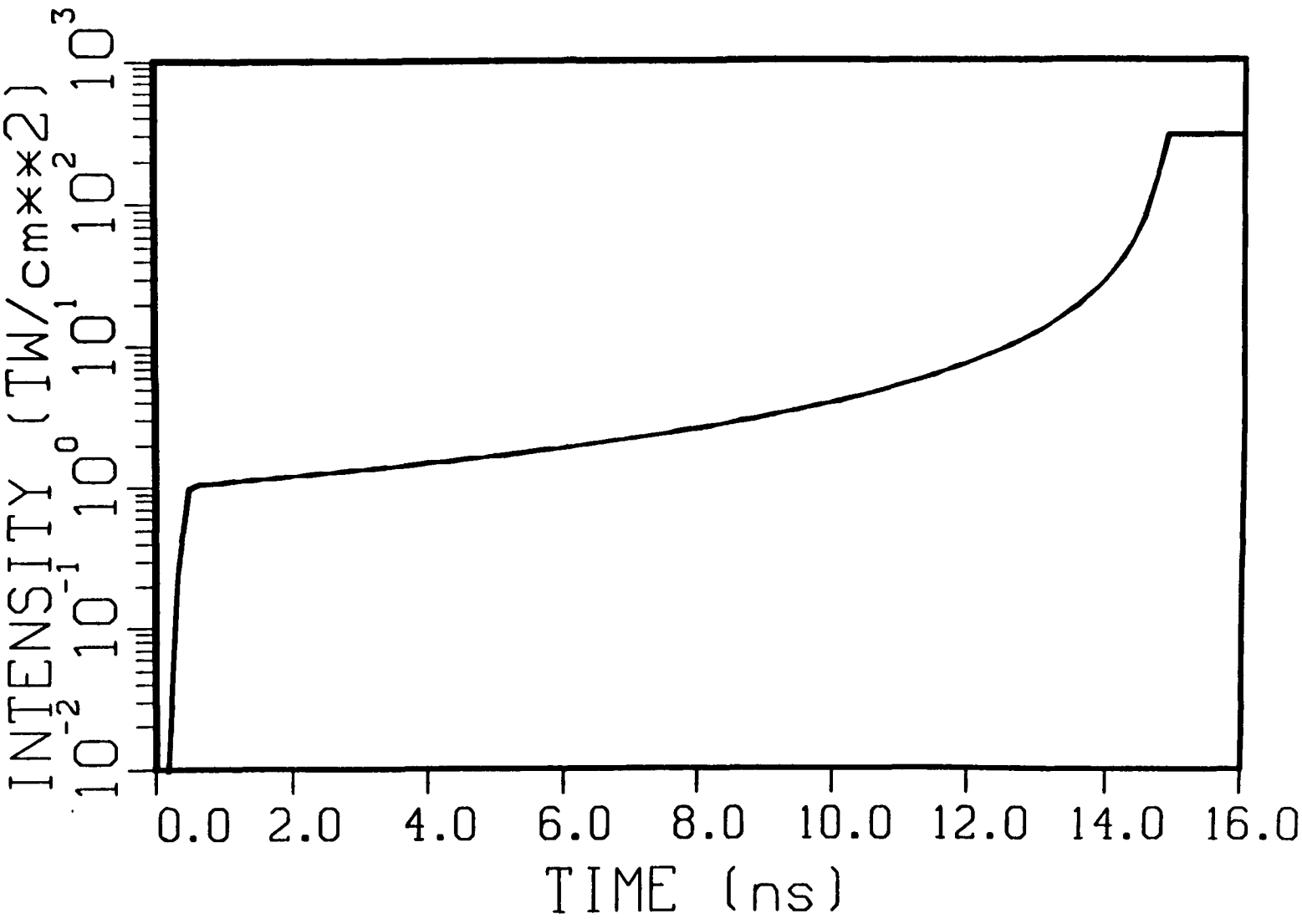

8. Temporal variation of a shaped power law laser pulse.

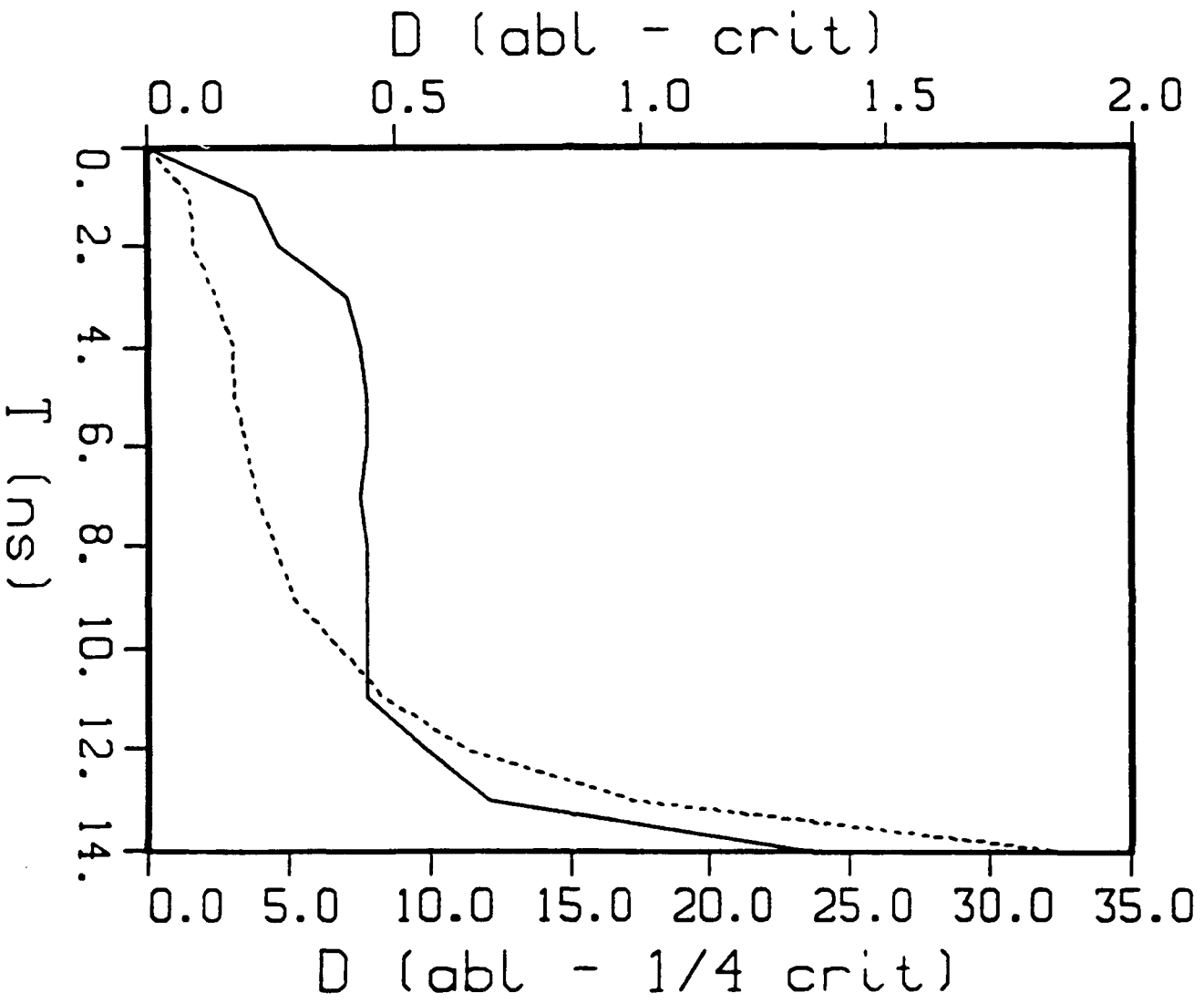

9. Plot of the distance between the ablation surface and the critical surface (solid line) and the distance between the ablation surface and the quarter critical surface (dashed line), in microns, versus time for the shaped power law laser pulse illustrated in Figure 8.

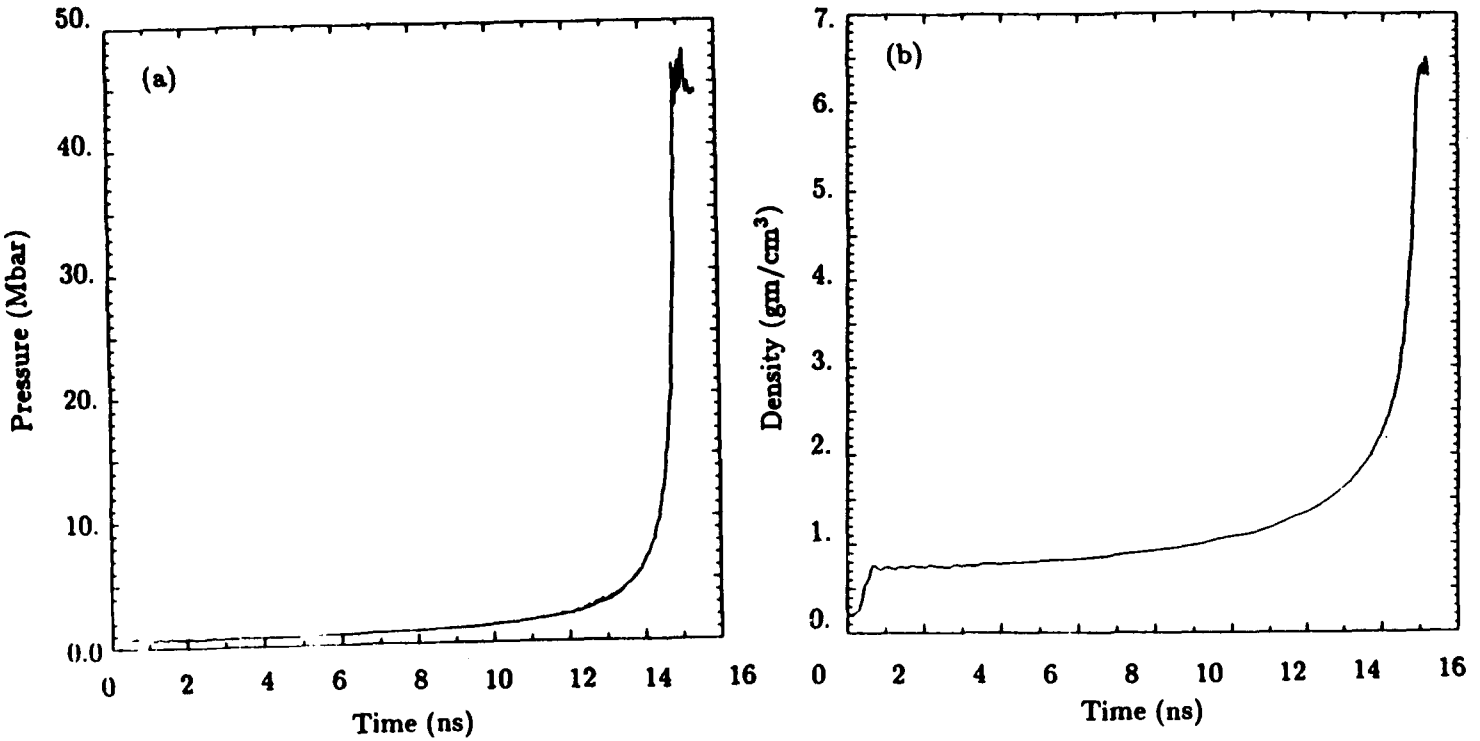

10. Plots of the ablation pressure (a) and peak target density (b) versus time for a 330 μm thick frozen DT target illuminated with the laser pulse shown in Figure 8.

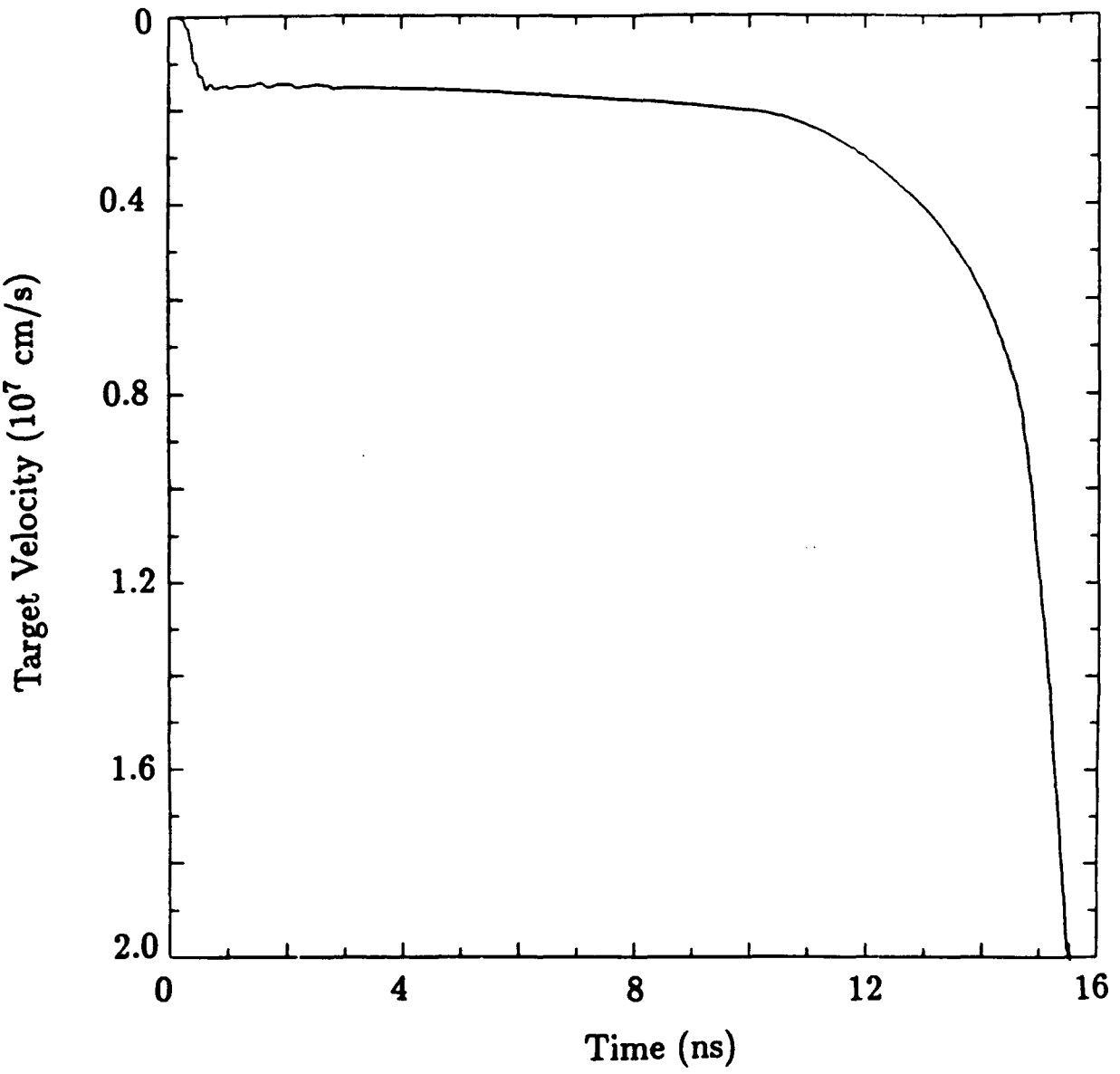

11. The velocity history of the target illustrated in Figure 10.

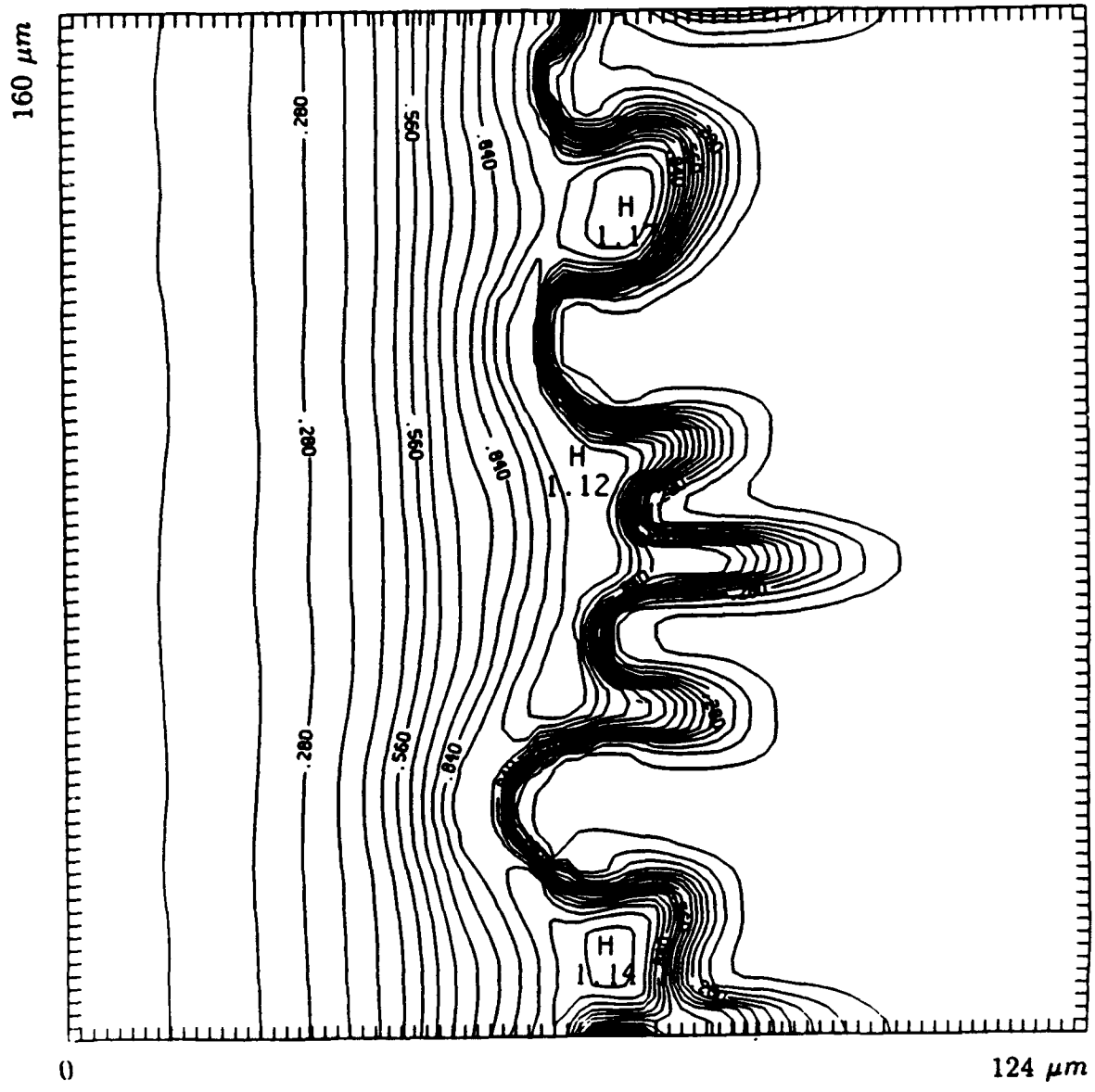

12. Isodensity contours at 12 ns for a 330 μm thick DT target illuminated with a 0.264 μm ISI laser beam with a power law time dependence. The horizontal dimension is 124 μm and the transverse dimension is 160 μm.

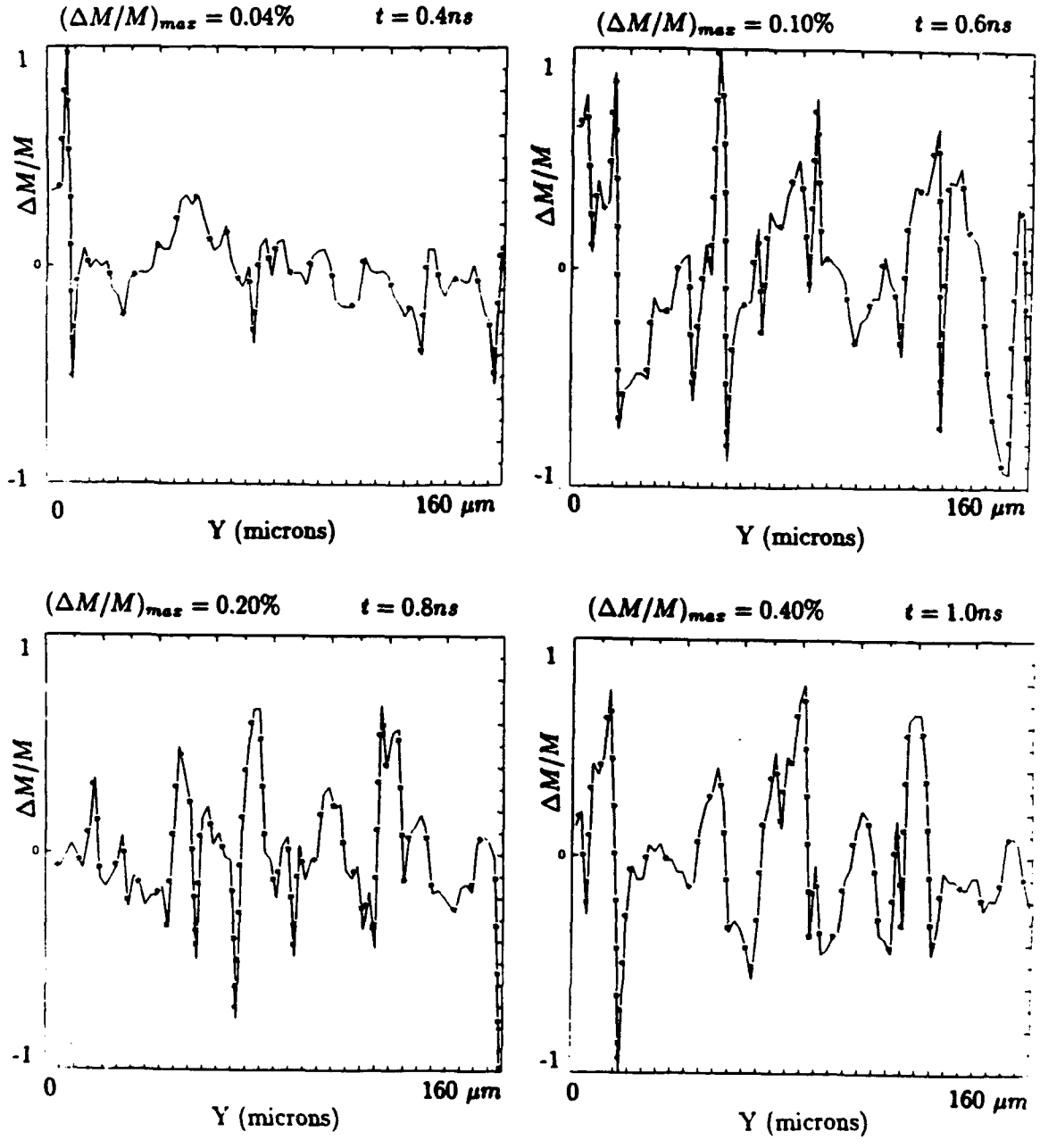

13. Plots of the total mass variation $\Delta M/M$ versus the transverse dimension (in microns) at 0.4, 0.6, 0.8, 1.0 ns showing the rapid oscillations in the mass perturbations as the shock impacts the target. $\Delta M/M$ has been normalized to 1 for each time.

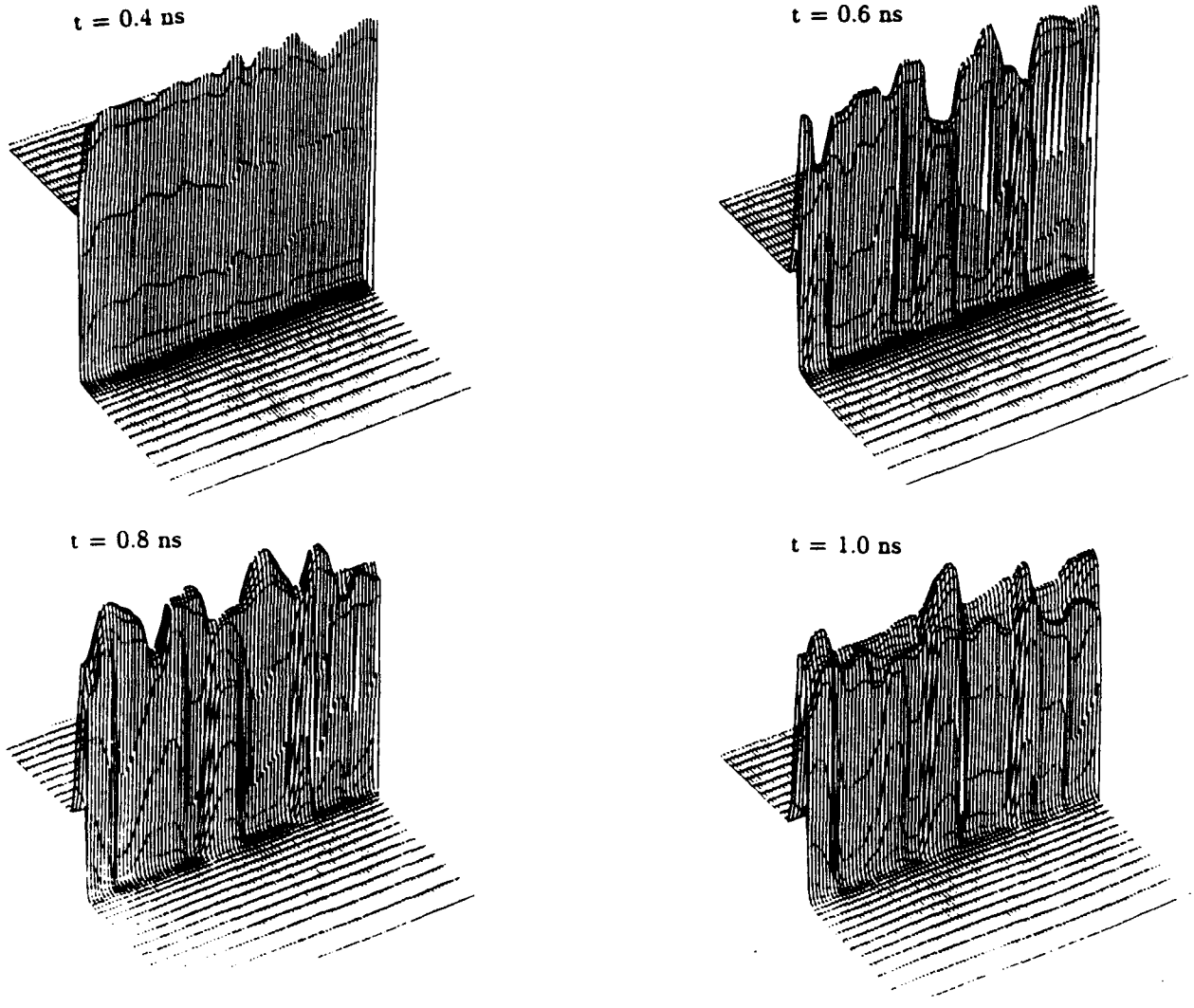

14. 2D perspective plots of the target mass density at the same 4 times as in Figure 13. The laser is impacting the target from the front. The vertical dimension is linear.

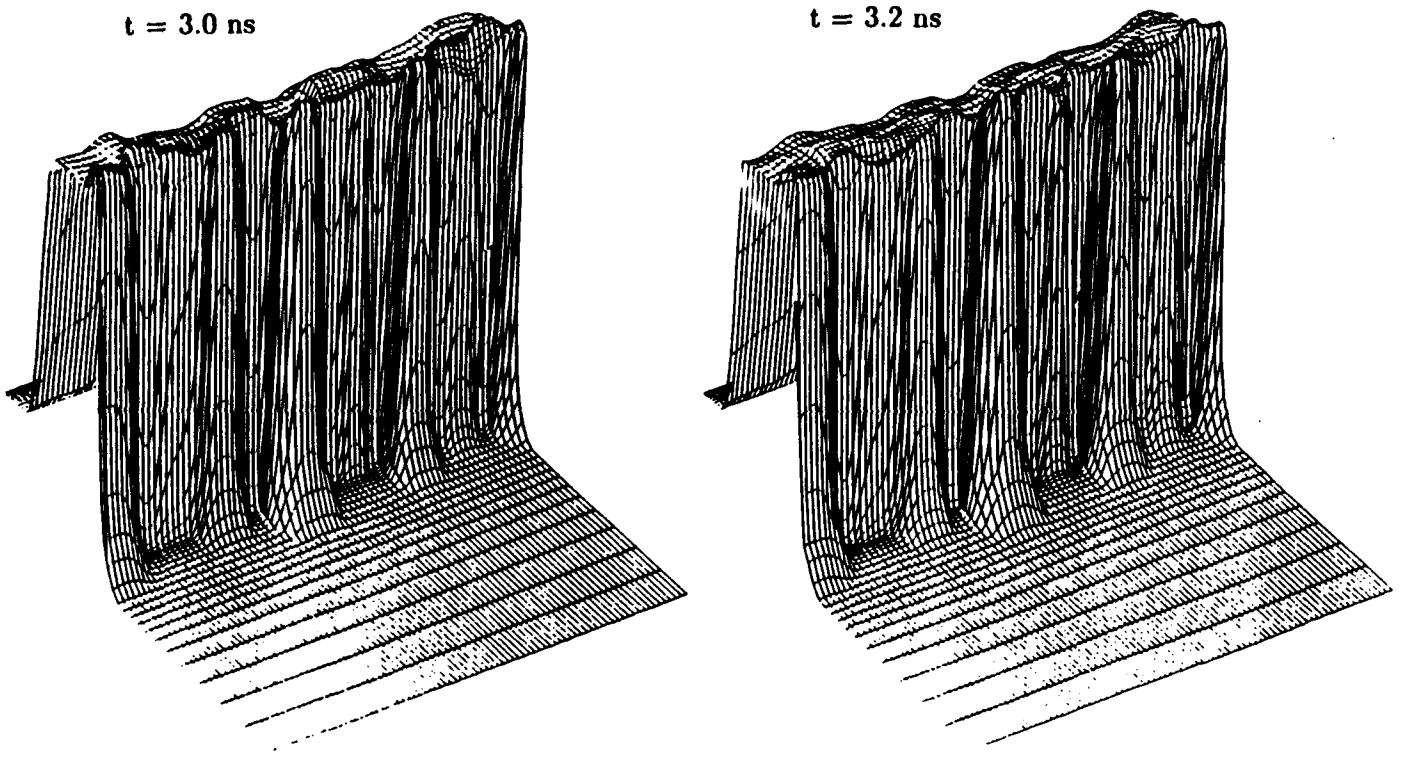

15. 2D perspective plots of the target mass density at 3.0 and 3.2 ns showing little change in the mass variation at this time.

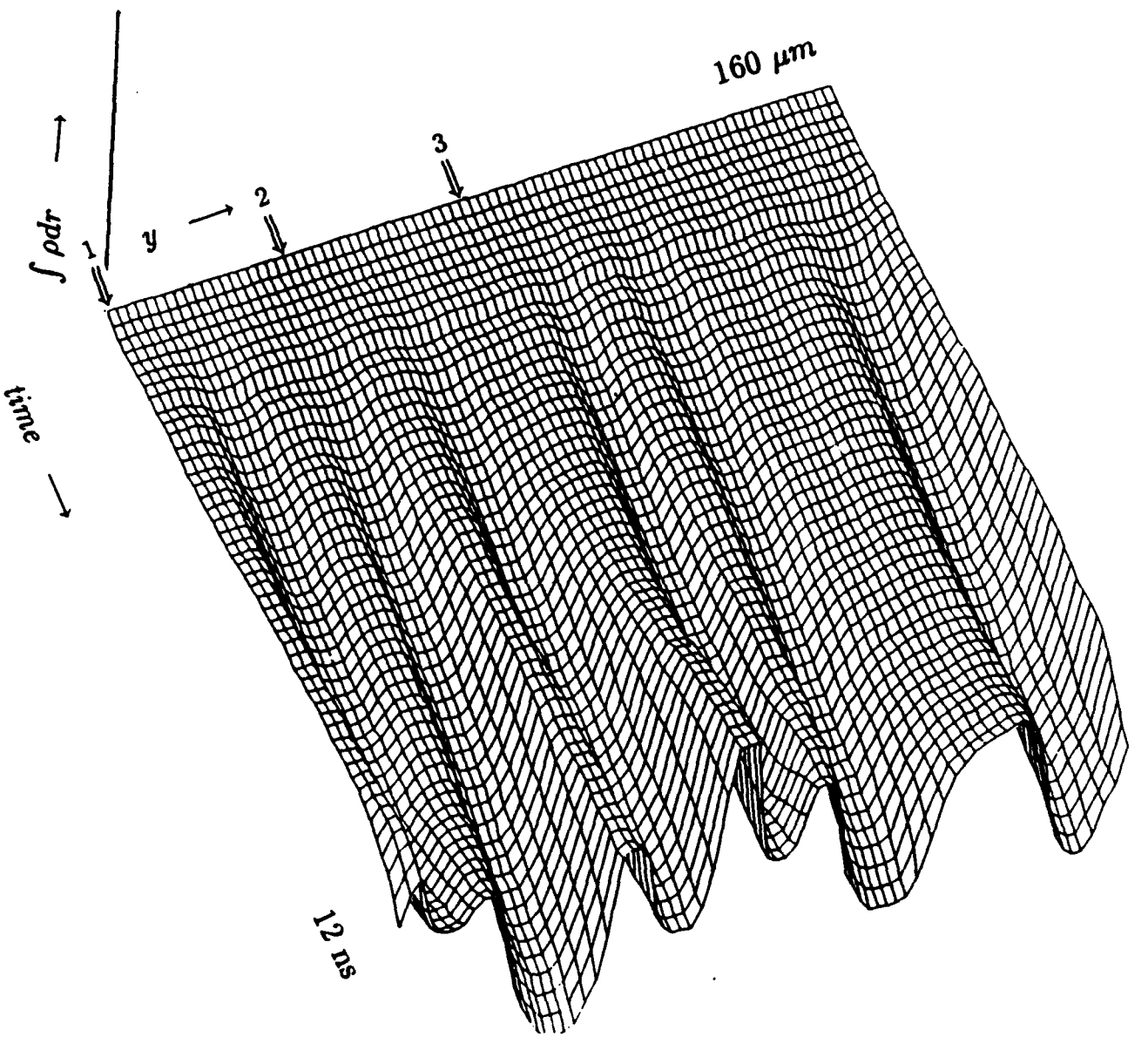

16. A 2D surface plot of the integrated mass density ρr versus the transverse target dimension (microns) as a function of time (ns).

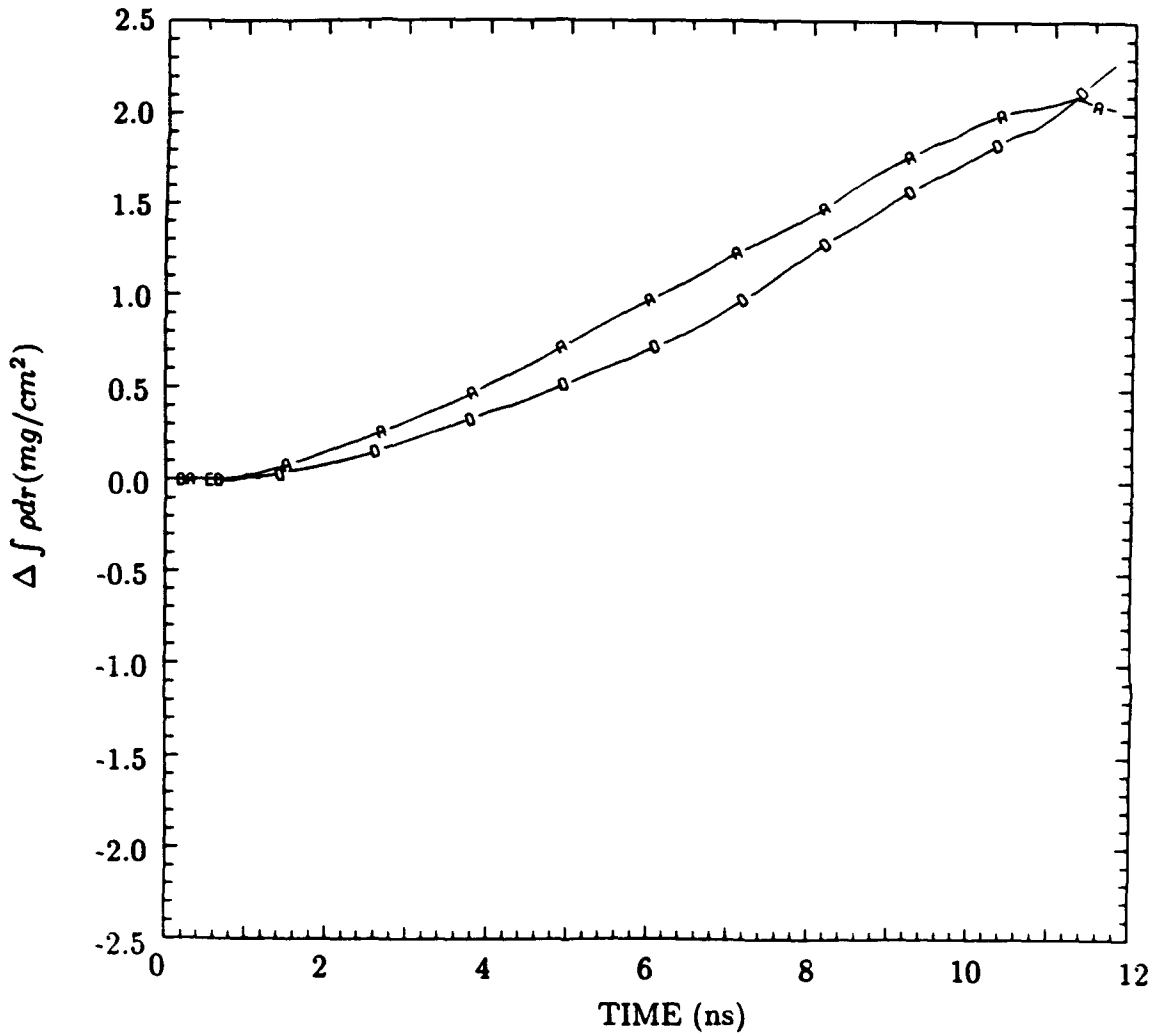

17. $\Delta\rho r$ between lineouts taken along paths 1 and 2 and along paths 2 and 3 (see Figure 16) plotted as a function of time. The initial growth is linear in time.

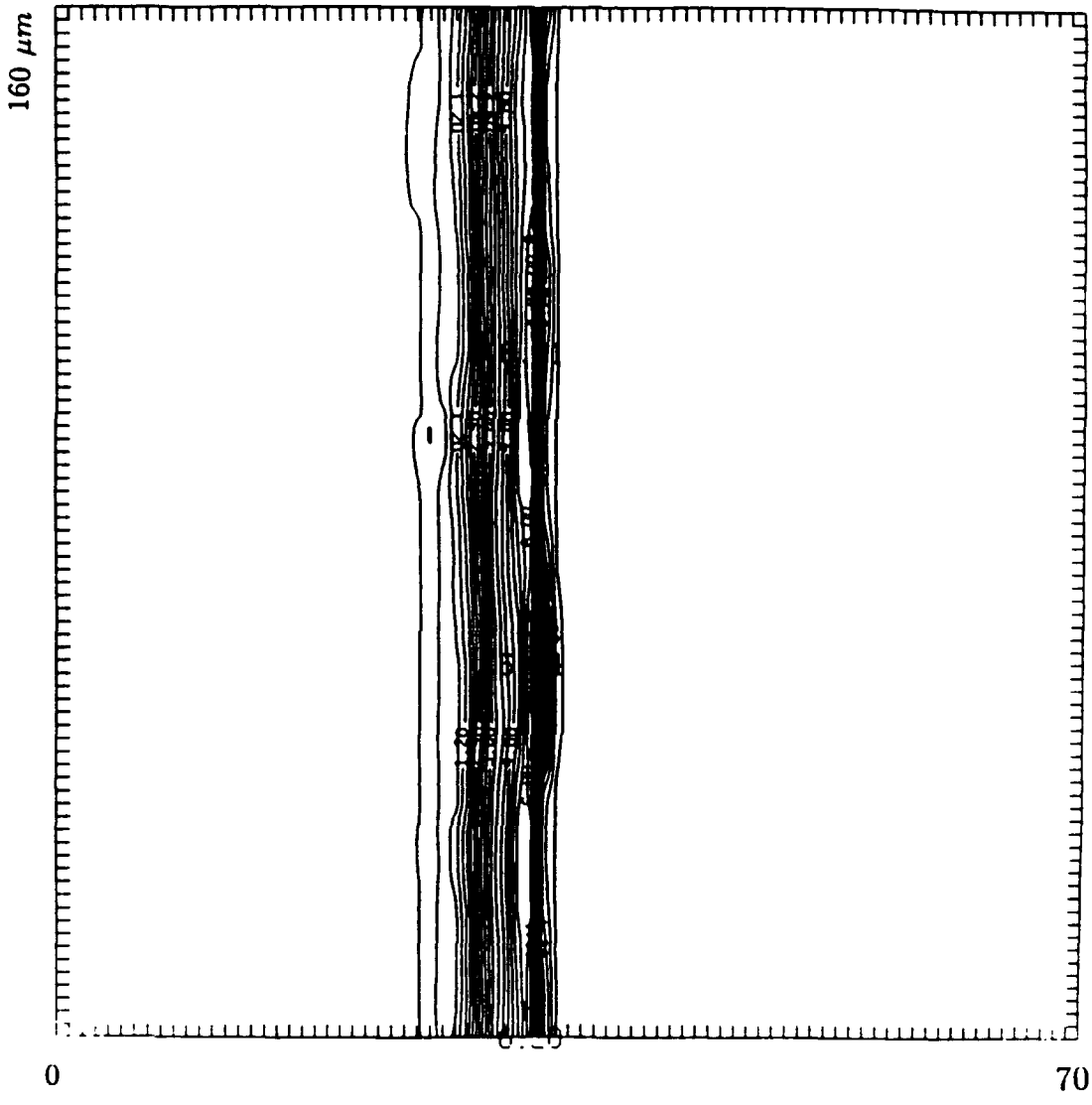

18. Isodensity contours at 15 ns for 180 μm frozen DT target with a 100 μm low density layer illuminated with "perfect" 1 μm laser light between 0 - 8 ns and ISI-smoothed 1/4 μm laser light between 8 - 15 ns.

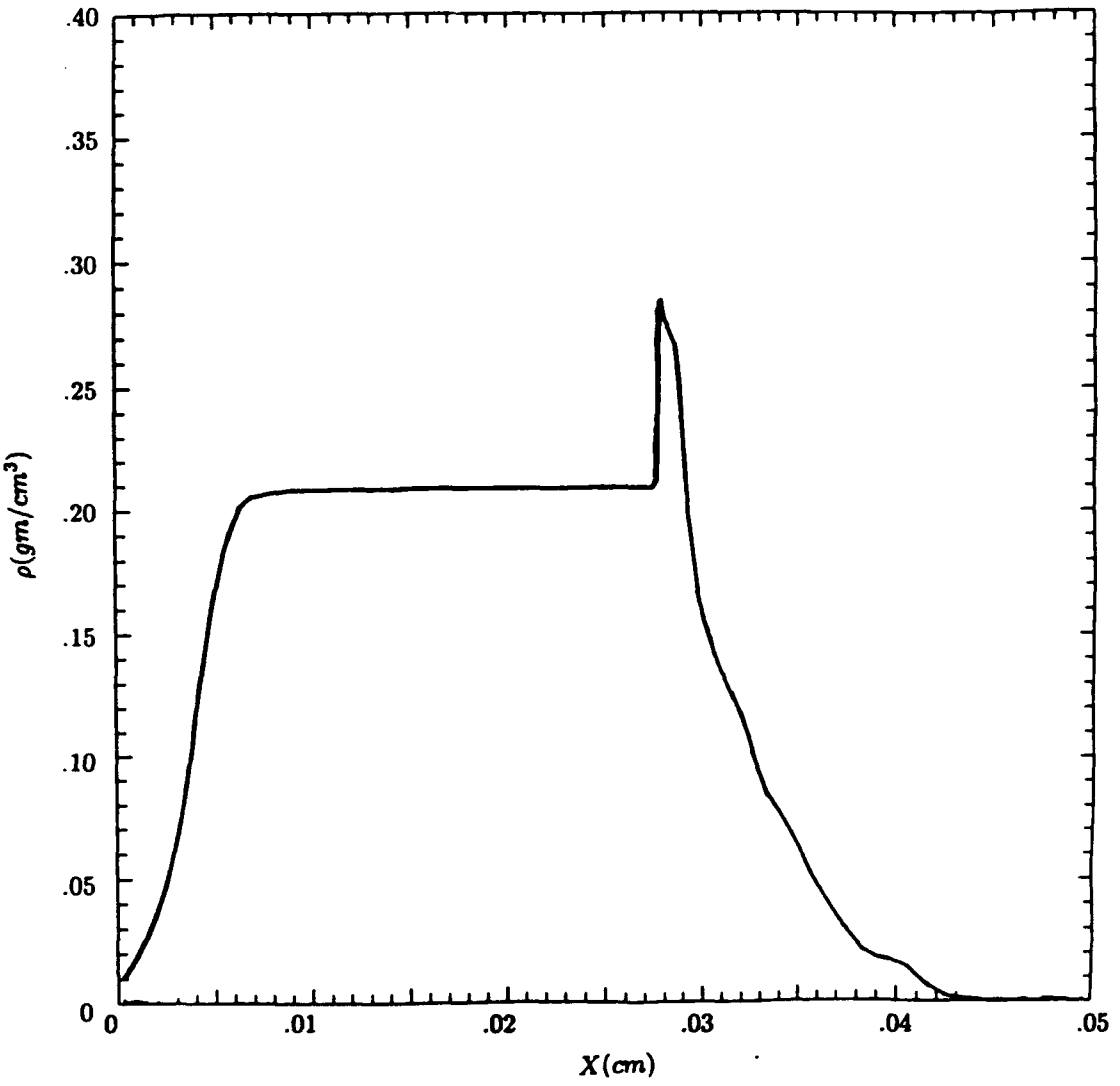

19. Density profile of 330 μm thick DT target 10 ns after being illuminated with an artifical 250 ps "x-ray flash".

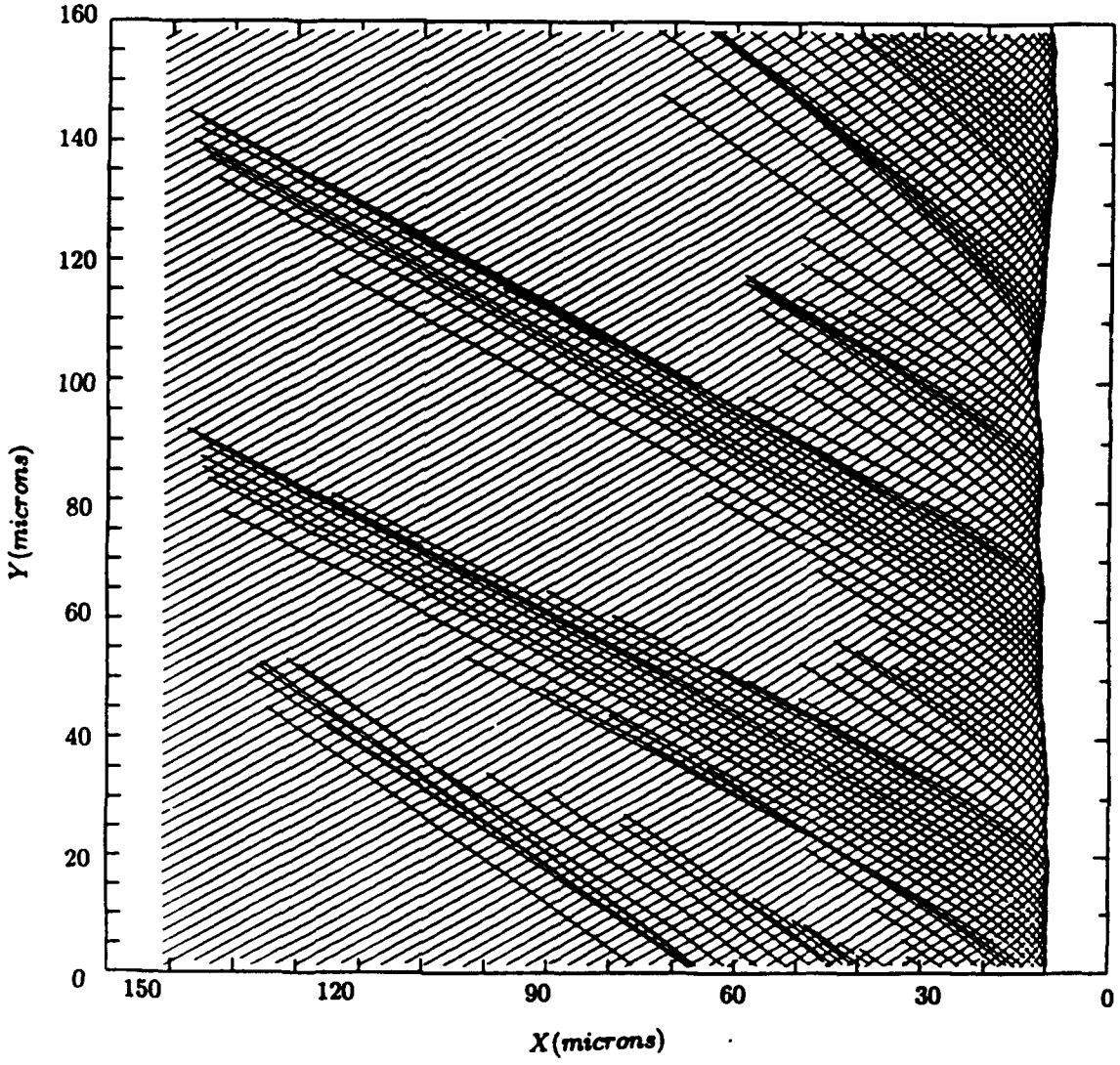

20. Plot of the rays incident at an angle of 30° at the peak of the laser pulse. The horizontal and vertical dimensions are in microns.

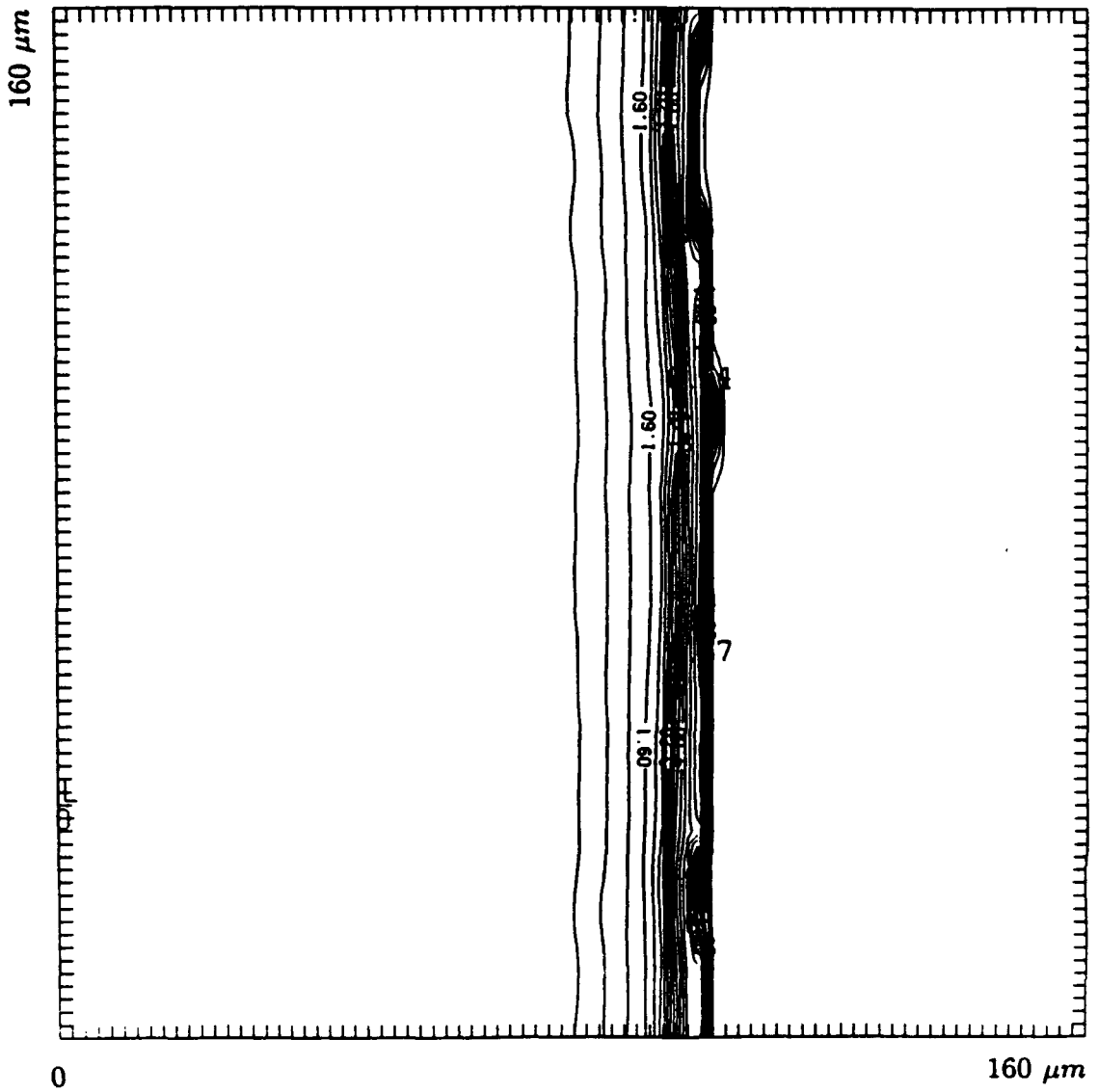

21. Isodensity contours for the 30° angle of incidence case at the peak of the laser pulse. The horizontal and vertical dimensions are both 160 μm.